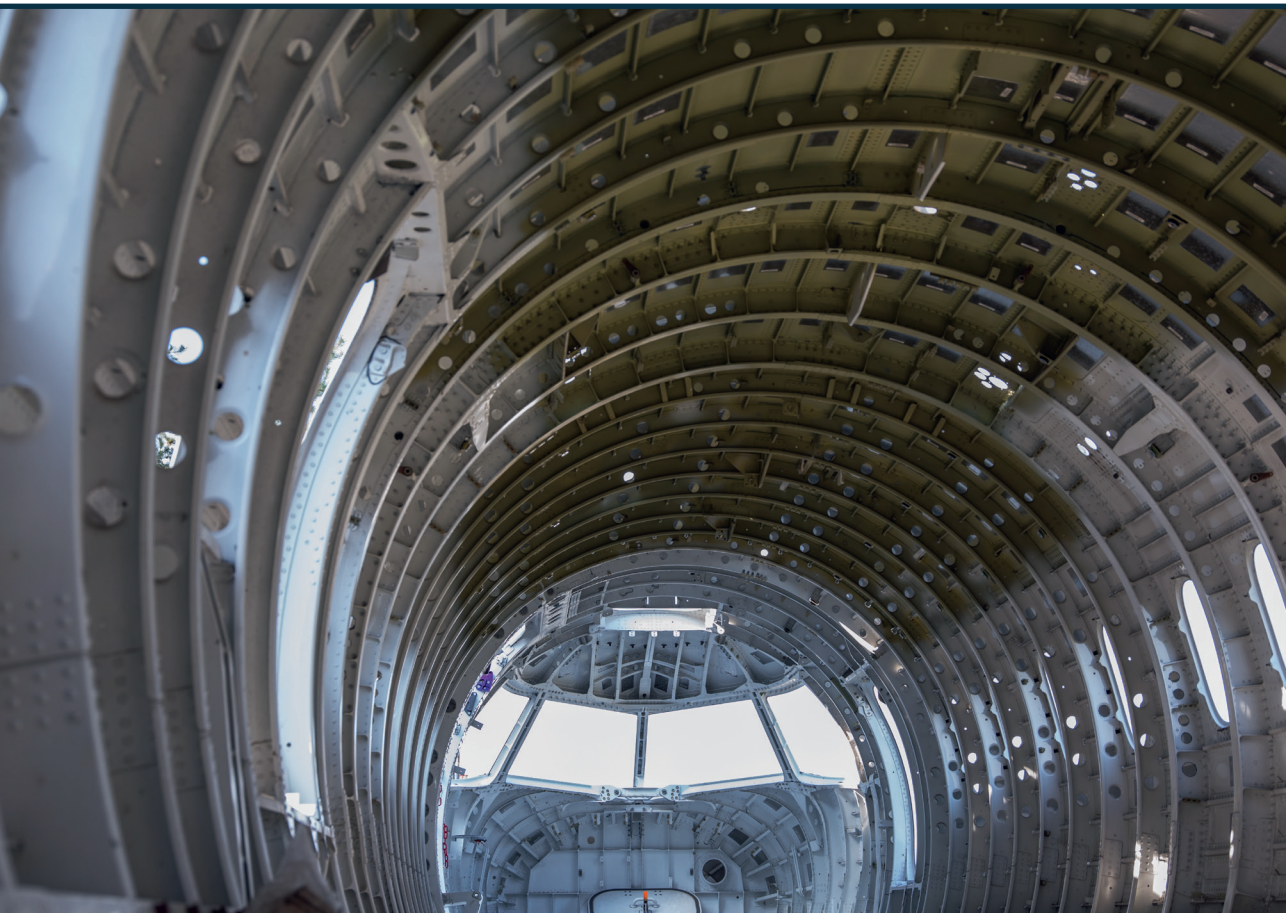


Pavithra Nagaraj

**STUDY OF FATIGUE DAMAGE DETECTION
BY CURRENT INFORMATION
OF MEASUREMENT SYSTEM**

Summary of the Doctoral Thesis



RIGA TECHNICAL UNIVERSITY

Faculty of Mechanical Engineering, Transport and Aeronautics
Institute of Aeronautics

PAVITHRA NAGARAJ

Doctoral Student of the Study Programme “Aviation Transport”

**STUDY OF FATIGUE DAMAGE DETECTION
BY CURRENT INFORMATION
OF MEASUREMENT SYSTEM**

Summary of the Doctoral Thesis

Scientific Supervisor:

Professor Dr. habil. sc. ing.
VITĀLIJS PAVELKO

RTU Press
Riga 2023

Nagaraj P. Study of Fatigue Damage Detection by Current Information of Measurement System. Summary of the Doctoral Thesis. – Riga: RTU Press, 2023. – 48 p.

Published in accordance with the decision of the Promotion Council “RTU P-22” of 28 June 2023, Minutes No. 04030-9.16.1/7.

<https://doi.org/10.7250/9789934229978>
ISBN 978-9934-22-997-8 (pdf)

DOCTORAL THESIS PROPOSED TO RIGA TECHNICAL UNIVERSITY FOR THE PROMOTION TO THE SCIENTIFIC DEGREE OF DOCTOR OF SCIENCE

To be granted the scientific degree of Doctor of Science (Ph. D.), the present Doctoral Thesis has been submitted for the defence at the open meeting of RTU Promotion Council on December 1st, 2023 at 13.00 p. m. at the Faculty of Mechanical Engineering, Transport and Aeronautics of Riga Technical University, Ķīpsālas Street 6b, Room 513.

OFFICIAL REVIEWERS

Dr. sc. ing. Sandris Ručevskis,
Riga Technical University

Ph. D. Wolfgang Grill
University of Leipzig, Germany

Dr. habil. sc. ing. Sergey Ignatovich
National Aviation University, Ukraine

DECLARATION OF ACADEMIC INTEGRITY

I hereby declare that the Doctoral Thesis submitted for the review to Riga Technical University for the promotion to the scientific degree of Doctor of Science (Ph. D) is my own. I confirm that this Doctoral Thesis had not been submitted to any other university for the promotion to a scientific degree.

PAVITHRA NAGARAJ.....(signature)

Date:

The Doctoral Thesis has been written in English. It consists of an Introduction; 4 Chapters; Conclusion; 71 figures; 7 tables; the total number of pages is 103. The Bibliography contains 102 titles.

CONTENTS

INTRODUCTION.....	5
The topic relevance	5
The aim and objectives of the Doctoral Thesis.....	6
Novelty of scientific research	7
Practical application of the Thesis	7
Thesis structure and its main results.....	7
Research methodology.....	9
Publications and Thesis approbation.....	10
Author’s contribution to publications	10
CHAPTER 1. OVERVIEW: ULTRASONIC METHODS IN SHM, LATEST ADVANCEMENT AND STATE-OF-THE-ART RESEARCH REVIEW	11
CHAPTER 2. OWN STRENGTH OF PIEZOELECTRIC TRANSDUCER FOR SHM...	12
CHAPTER 3. ACTIVE METHODS OF SHM USING ULTRASOUND TECHNIQUES	19
CHAPTER 4. OTHER APPLICATIONS: LOAD MONITORING AND ACOUSTIC EMISSION.....	29
5. GENERAL CONCLUSIONS.....	46
6. BIBLIOGRAPHY	47

INTRODUCTION

The topic relevance

The ultrasonic diagnostic technologies have found wide application in civil, medicine, aerospace, and many other areas. As a basic principle of measurement, the ultrasonic method is one of the most naturally adapted for use in structural health monitoring (SHM) systems. The significant advantage of the ultrasonic method is the possibility of multi-optional applications (classical damage detection, guided wave technology, electromechanical impedance technology, stress, and load measurement). Each of those options can be optimally applied in some specific conditions, but the combined application can also be realised.

However, there are several problems that negatively influence the reliability of results and effectiveness of in-built monitoring. First, it is the problem of the mechanical strength and lifetime of sensitive elements of the SHM system. In contrast to non-destructive testing (NDT) those elements of the SHM system are in-built to monitor the structure and subjected to the same operational load and environmental actions as the host component of a structure. Degradation processes can cause partial or full loss of operability of SHM system. The problem can be solved partly by protecting sensitive elements from negative external actions. Another way to increase the reliability of monitoring is to use the so-called “reference-free” approach to evaluation of the damaged state of a structural component. This approach joins options in which the technical condition assessment is based on current or accumulated information, without reference to the initial state (baseline). For the case of fatigue cracks, it is known that the response of the ultrasonic monitoring system is different for a mechanically loaded state (the crack is open) and an unloaded one (the crack is closed). The response of the second state can be taken as the current baseline.

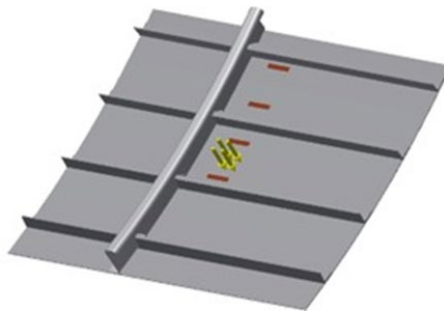


Fig.1. The typical part of metallic fuselage equipped with piezoceramic transducers.

In the present work, the relevant problems of realisation of mentioned approach are investigated for a skin of the hermetic part of metallic fuselage (Fig. 1). In the cruising flight, the skin is statically loaded by internal air pressure in the cabin, but after landing the skin is unloaded.

Obviously, load monitoring involves an indirect way to assess the structural health of a structure. This estimate can be obtained based on the use of an acceptable generalised damage parameter determined by the results of load monitoring and its comparison with the strength characteristics of the controlled structural element. A critical value of the damage index may be established in accordance with the safety factor approach.

An alternative is the probabilistic approach. Both compared quantities are random. Therefore,

the damage index should have a probabilistic formulation and be perceived as a requirement for additional verification and assessment of the technical condition of the structural element in question. The procedure of this type is developed in the Thesis, and its fundamental fragment is presented.

A similar use case for the passive response of a piezoelectric transducer provides acoustic emission monitoring. It can be effectively used in endurance fatigue tests.

So, all the mentioned problems directly influence the operability and reliability of ultrasonic SHM systems. Their investigation and solution are relevant to nowadays applied science.

The aim and objectives of the Doctoral Thesis

The general aim of the research. Solutions for several relevant problems of operability and reliability of ultrasonic structural health monitoring mainly using the current information of embedded piezoceramic transducers working in active and passive regimes of damage detection.

The following objectives should be solved for the achievement of the formulated general aim:

1. Analysis of the piezoceramic transducer strength using Internet resources, experimental data, and finite element analysis (FEA) of stress state for typical installation and typical operational loading. Development of recommendations for prevention of damages at the static and cyclical load.
2. Estimation of electromagnetic interference (EMI) as the primary method of fatigue crack detection, comparison of properties of alternative indices of damage, and the development of the detailed procedure of measurement data processing.
3. Investigation of the crack open/close effect on EMI and estimation of this effect suitability for the crack-type damage detection.
4. Improvement of the damage indices for the crack-type damage detection by the guided wave technology using fatigue test data and simulation outcome.
5. Demonstration of application of the references-free virtual system of SHM (for the skin of hermetic fuselage of aircraft)
6. Analysis of piezoelectrical transducer application for load monitoring. Development of the fatigue damage index with the use of the rain-flow method of operational load transformation and concept of safety factor.
7. Probabilistic model of strength for SHM of a lifetime by using load monitoring.
8. Analysis of acoustic emission (AE) application as a passive ultrasonic method with respect to its use in laboratory tests of aircraft full-scale components.

Novelty of scientific research

1. Novel statistical characteristics on the fatigue lifetime of typical piezoceramic transducers were found.
2. General properties of the stress state of piezoceramic transducers at different options of their embedding into the monitored structural component and recommendations on the providing of strength at operational load.
3. The crack open/close effect on the ultrasonic index of damage as the theoretical base of the reference-free SHM system which uses the current data of the transducer only.
4. Novel procedure of EMI measurements processing which includes selecting the width of the data set window and defining the frequency band of highest stability of damage index.
5. New damage index for fatigue crack detection using guided wave technology (GWT). This index is the convolution of response using the excitation signal as the mother function.

Practical application of the Thesis

1. The obtained realistic estimates of the strength and the fatigue lifetime of a typical piezoceramic transducer are useful for designing the PZT-based SHM system.
2. The improved procedure of processing EMI measurement can raise the trustworthiness of damage detection.
3. The proposed index of damage for GWT of SHM provides higher reliability and accuracy of structural damage detection.
4. The example of a hypothetical SHM system for the skin of a hermetic fuselage can be useful in the design of a local SHM system.
5. Direct simulation of the response of piezoceramic transducer as an important stage of its use of load (stress) monitoring.
6. Basic technical requirements for bench testing and full-scale real-time testing of helicopters using acoustic emission (AE) as a passive ultrasound method have been formulated. It can be effectively used in endurance fatigue tests.

Thesis structure and its main results

The Thesis comprises 4 chapters.

In Chapter 1, the overview of ultrasonic methods, the latest advancement and state-of-the-art research are reviewed.

In Chapter 2, the own mechanical strength of piezoelectric transducers and their connection with the monitored host structure as the primary problem of reliability of SHM of aircraft structures are analysed and summarised in publication No. 4, with the three main topics covered:

1. More detailed description of the problem.

2. Essential results of transducer destruction during the fatigue test.
3. Investigation of the stress state of transducers embedded in the thin-walled structure.

In Chapter 3, active methods of SHM using ultrasound techniques are analysed and summarised in publications No. 3 and 4 with the main topics covered:

1. Electromechanical impedance, its components, and EMI parameters.
2. Other indices of EMI-based system of SHM.
3. Experimental study of the crack open/close effect and the perspective of its use in SHM.
4. Aim of experimental investigation.
5. The test sample, equipment, and test setup.
6. Essential outcomes of the experiment.
7. Application to the SHM of the skin of hermetic fuselage is analysed. demonstration of impedance-based SHM of the hermetic fuselage skin.
8. Predictions of fatigue crack growth and estimation of lifetime.

In Chapter 4, other applications – load monitoring and acoustic emission – are analysed in some unpublished results, and publications No. 1 and 2 are summarised, with five topics covered:

1. Related applications.
2. Load monitoring using piezoelectric transducer (PZT) response.
3. Equivalent stress and structural health assessment by use of load(stress) monitoring.
4. Probabilistic model of strength for SHM of a lifetime using load monitoring.
5. Acoustic emission as a passive method of ultrasound techniques.

The Following conclusions are drawn:

1. A complete analysis was made of the piezoceramic transducer strength using Internet resources, experimental data, and finite element analysis (FEA) of stress state for typical installation and typical operational loading. Recommendations for the prevention of damages to the static and cyclical load are made.
2. Estimation of EMI as the primary method of fatigue crack detection is made. The comparison is made of properties of alternative indices of damage. The detailed procedure of measurement data processing is developed.
3. The crack open/close effect on EMI is investigated, and the suitability of this effect for the crack-type damage detection is estimated.
4. The two improved damage indices for the crack-type damage detection by the guided wave technology are developed. Both damage indices (root-mean-square deviation (RMSD) and time-of-flight) are based on the convolution of the response signal for which the excitation signal is used as the mother function.
5. The example of the application of the reference-free virtual system of SHM is demonstrated (for the skin of the hermetic fuselage of the passenger aircraft). It can be concluded that a hermetic fuselage structure is a very convenient field for the application of ultrasonic technology for structural health monitoring which uses the crack open/close effect.
6. The application of a piezoelectrical transducer for load monitoring is analysed. The fatigue damage index with the use of the rain-flow method of operational load counting, fatigue test data and simulation outcome developed. The allowable value of index is mainly defined by the safety factor.
7. Probabilistic model of strength for SHM of a lifetime by using load monitoring is presented. Using this model, it is possible to solve the problem of the proper determination of the maximum allowable parameter or diagnostic sign for indication in the cockpit when the predetermined limit of its actual value is known in advance.

8. The application of acoustic emission (AE) as a passive ultrasonic method is analysed in respect of its use in laboratory tests of aircraft full-scale components. Basic technical requirements of bench tests for real-time full-scale testing of helicopters are formulated. The results obtained from bench tests can be used in testing calculations of the resources of helicopter elements according to the criteria of short-term strength and endurance.

Research methodology

The research is studies fatigue damage detection using the piezoelectric phenomenon of transducers. The study is focused on active methods and passive methods of guided wave propagation. First, experimental methods of fatigue damage destruction were conducted. In this experiment, the task was to assess the fatigue strength of the panel and the effectiveness of the monitoring system based on the Lamb wave technology. For this purpose, two groups of five piezoelectric transducers PIC 151 with dimensions of $0.5 \text{ mm} \times 10 \text{ mm} \times 50 \text{ mm}$ were installed on the surface of the lining parallel to the axis of the stringer on each side. At the stage of initiation of the fatigue crack, the technical condition of the transducers periodically (after 20 thousand cycles) was monitored by measuring their electromechanical impedance and comparing it with its value before the start of the tests (baseline).

Secondly, finite element analysis was executed by using the COMSOL Multiphysics software of the study option Stationary. Because there is double axial symmetry of the model in the coordinate plane xz, the outcome of stress analysis is presented for one- quarter part of the model. The general view is presented of the distribution of stresses (in the form of Von Mize's equivalent stress) and the deformed shape of the model at tensile longitudinal load were illustrated.

Thirdly, the modal analysis of the system "host structure – PZT" dynamic response is the basic tool of this model, and final EMI equations are derived. This model directly uses the results of modal analysis of structure and is independent from the details of structure configuration – boundary conditions and external loading, which is the main advantage of the EMI model. For this study the modal analysis is performed in COMSOL Multiphysics, and its results transmit to MATLAB in which the algorithm of the EMI model is realised.

To demonstrate the impedance-based SHM of the hermetic fuselage skin, the geometrical modelling is carried out in *Autodesk Inventor*.

To solve the problem of piezoelectricity for any linear piezoelectric device in a constitutive relation in the tensorial form, sensing piezoelectrical equations in compressed form are used.

Using the Gaussian law of distribution, the mathematical model for the probabilistic approach to the construction of the fatigue damage index is analysed.

Publications and Thesis approbation

The proceedings of conferences contain the complete texts of papers indexed in SCOPUS and the Web of Science.

1. Urbaha, M., Carjova, K., Nagaraj, P., Turko, V. Requirements for Helicopter's Planer Construction Fatigue Testing. In: Transport Means 2018: Proceedings of the 22nd International Scientific Conference, Lithuania, Trakai, 3–5 October 2018. Kaunas: Kaunas University of Technology, 2018, pp. 1268–1270. ISSN 1822-296X. e-ISSN 2351-7034.
2. Nedelko, D., Urbahs, A., Urbaha, M., Carjova, K., Turko, V., Nagaraj, P. Assessment of the Limits of Signs of Health, and Usage Monitoring System for Helicopter Transmission. *Procedia Computer Science*, 2019, Vol. 149, pp. 252–257. ISSN 1877-0509. Available from: Doi: 10.1016/j.procs.2019.01.131.
3. Nagaraj, P., Pavelko, V. Crack Open/Close Effect on Impedance Based System of Structural Health Monitoring. In: *TRANSBALTICA 2022: TRANSBALTICA XIII: Transportation Science and Technology*. Lithuania, Vilnius, 15–16 September 2022. Lithuania: Springer, Cham, 2023, pp. 797–805. ISBN 978-3-031-25866. e-ISBN 978-3-031-25863-3. Available from: Doi:10.1007/978-3-031-25863-3_78
4. Pavelko, V., Nagaraj, P. “On the combined system of structural health monitoring (SHM) of the skin of the fuselage sealed part”. Seminars in Warshaw, Poland, November 2022, article in print.

Author's contribution to publications

All scientific publications have been written in collaboration with supervisors Professor Vitālijs Pavelko and the late Director Professor Aleksandrs Urbahs and with co-authors and consultants of publications. The work on scientific publications was collectively planned and accomplished by the authors.

CHAPTER 1.

OVERVIEW: ULTRASONIC METHODS IN SHM, LATEST ADVANCEMENT AND STATE-OF-THE- ART RESEARCH REVIEW

The fact that SHM sensors and actuators are permanently attached to the structure, as opposed to typical NDT systems, allows the system to gather data virtually constantly for the duration of the structure's service life without human interaction. Typically, the system needs a very large number of sensors dispersed throughout the building to be helpful. This vast amount of data needs to be analysed continuously and automatically, reduced to warnings for the user (an aircraft engineer or maintenance specialist) when an overload is happening, when damage is discovered, or to create cumulative fatigue reports of the structure. [1]

Recent advancements in piezoelectric transducers for SHM applications include:

1. Smart piezoelectric materials. New types of piezoelectric materials have been developed that can adapt to their environment, leading to better performance and reliability in varying conditions. For example, piezoelectric materials that can self-diagnose and repair small cracks have been developed, which can improve the longevity of the transducer.
2. Flexible piezoelectric transducers. Flexible and conformable piezoelectric transducers have been developed, which can conform to complex surfaces and improve the accuracy of defect detection in curved or irregular geometries.
3. Multi-functional piezoelectric transducers. These transducers can perform multiple functions, such as sensing, actuation, and energy harvesting. For example, piezoelectric transducers that can generate power from vibrations in the structure have been developed, which can be used to power the SHM system or other devices on the aircraft.
4. Non-contact piezoelectric transducers. Non-contact piezoelectric transducers that do not require physical contact with the structure have been developed. These transducers use air-coupled ultrasonic waves to detect defects in the structure, which can be useful for inspecting composite materials or structures that are difficult to access.

Overall, these advancements in piezoelectric transducers have the potential to improve the accuracy, reliability, and efficiency of SHM systems for aviation and other applications.

While piezoelectric transducers (PZT) are widely used and have seen many advancements, there are still several challenges and problems that need to be addressed in PZT technology, including:

1. Temperature stability. PZT materials exhibit changes in their piezoelectric properties as temperature changes, which can lead to measurement errors in SHM applications. Improving the temperature stability of PZT materials is an ongoing challenge.
2. Environmental robustness. PZT materials are sensitive to moisture and other environmental factors that can cause degradation over time. To improve the longevity and reliability of PZT transducers, researchers are exploring new coatings and packaging materials that can protect the transducer from harsh environments.
3. Sensitivity to bonding. PZT transducers are typically bonded to the structure using adhesives,

and the bonding process can affect the transducer's performance. Researchers are exploring new bonding techniques that can improve the coupling between the transducer and the structure and reduce the impact of the bonding process on the transducer's performance.

4. Nonlinear behaviour. PZT materials exhibit nonlinear behaviour when subjected to high-amplitude signals, which can lead to distortion and other measurement errors. Researchers are exploring new signal processing and data analysis techniques that can account for the nonlinear behaviour of PZT transducers.

Overall, these challenges and problems highlight the need for continued research and development in PZT technology to improve the performance, reliability, and accuracy of PZT transducers in SHM applications.

CHAPTER 2.

OWN STRENGTH OF PIEZOELECTRIC TRANSDUCER FOR SHM

2.1. More detailed description of the problem

The problem of the own reliability of the elements of the health structural monitoring system is of the utmost importance. For monitoring systems based on the use of ultrasonic detection, this problem is especially relevant for piezoelectric transducers. It is known that these elements are built into the structure and in the process of operation are subjected to the same external influences as the host structure. First, it is a dynamic load, which can cause damage or complete destruction of the transducer during extreme overloads. Prolonged exposure to variable loads can lead to fatigue cracks in the sensitive elements of the transducers and their connection to the structure. Ageing processes of various nature, corrosion, and temperature effects can cause failures of transducers or partial loss of their functional performance. There are methods of prevention and protection against adverse external influences. But the most urgent is the problem of strength and fatigue durability of transducers. It is known that the most popular material of converters is piezoceramic. It is also known [2] that piezoceramics have sufficiently high compressive strength (about 600 MPa) and relatively low tensile strength (about 45 MPa) and bending (about 80 MPa). At the same time, to ensure effective detection of strength defects, transducers must be embedded in a structure that is most often exposed to tensile stresses. The simplest way to avoid sudden destruction or fatigue damage involves the installation of transducers on compressed or weakly loaded stretched sections of the structure. In any case, theoretical and experimental analysis of loading conditions and the establishment of safe loads for piezoceramic transducers are required. In [3] the conditions of loss of operability of a typical PZT installed on the surface of the bearing sample under static and fatigue loads are investigated. The results of the study can be used in relation to square-shaped transducers in the plane (7 mm × 7 mm) glued to a thin-walled structural element. The study in [4] presents the results of durability tests performed using embedded PZT transducers on composite panels under tensile static and cyclic loading. In [3], it is shown that the piezoceramic sensors still work well when they are bonded on the host structures with tensile strain up to 4000 $\mu\epsilon$ using the optimal adhesive. Another means of PZT protection from fatigue is proposed and developed in [5]–[6]. It is based on the creation in the transducer of a field of residual compressive stresses. Problems of strength and fatigue of piezoceramics under mechanical and electrical loads are analysed in [7].

This short overview shows that a special designing procedure should be accomplished to

provide reliable functioning of the PZT-based SHM system in operation. Investigation of strength problems of the rectangular shape of PZT is another specific aim of the analysis.

2.2. Essential results of transducer destruction during the fatigue test

In Fig. 2.1, an example of the aeronautical panel that contains a thin skin supported by a stringer of the angular cross-section is presented. Dimensions of the working part of the panel are: width 200 mm; length 380 mm; sheet thickness 1.15 mm. The stringer is made of a standard angular profile of 20 mm × 20 mm × 1.5 mm. The skin material is aluminium alloy 2024-T3. The material of the stringer is an aluminium alloy too.

The stringer has a longitudinal technological joint. The two parts of the stringer are connected to each other and to the skin by a rivet joint. In such a structure, an uneven distribution of shear forces on the rivets is inevitable, which is a potential cause for reduced fatigue strength. In this experiment, the task was to assess the fatigue strength of the panel and the effectiveness of the monitoring system based on the Lamb wave technology. For this purpose, two groups of five piezoelectric transducers PIC 151 with dimensions of 0.5 mm × 10 mm × 50 mm were installed on the surface of the lining parallel to the axis of the stringer on each side.



Fig. 2.1. A forced panel prepared for fatigue test and installed in machine GRM-20 (to the left) and the view of the panel after the penetration test (to the right) for finding the crack in PZT transducers.

Cyclic loading of the panel at a frequency of 10 Hz was carried out with a maximum stress of 150 MPa in the cross-section of the panel and minimum cycle stress of 50 MPa. At the stage of

initiation of the fatigue crack, the technical condition of the transducers periodically (after 20 thousand cycles) was monitored by measuring their electromechanical impedance and comparing it with its value before the start of the tests (baseline).

After 60000 cycles, EMI measurements showed that only three transducers remained fully operational. Five transducers were damaged (usually with several cracks) with a complete loss of functional performance. The remaining two transducers had no visible damage under the applied detection method used and partially retained the ability to respond to external excitation. However, the dynamic response to the excitation of the impact was significantly different from the baseline. The statistics of damages are shown in Table 1.

Figure 2.2 shows transducer No. 5 of the right group before the start of the fatigue test (left picture) and after their completion (right picture). On the surface of the transducer after the tests, traces of seven cracks are clearly visible, crossing the sensor across the entire width.

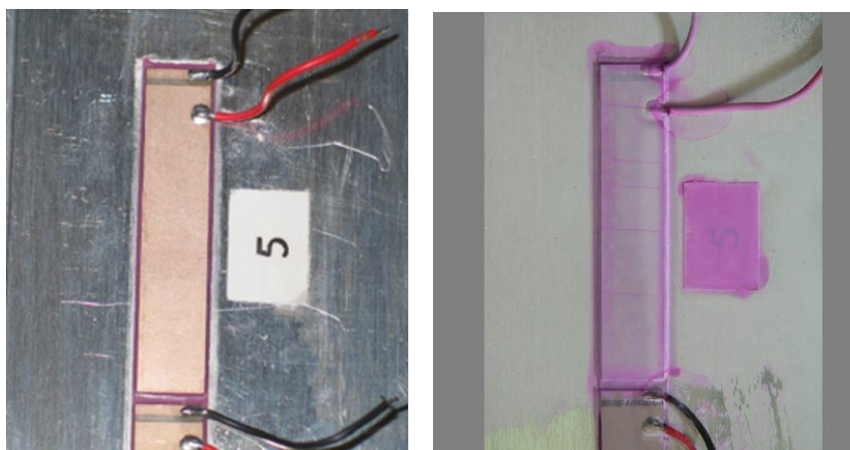


Fig. 2.2. View of PZT No. 5 before (left) and after (right) the fatigue test and cracks evaluation by the penetration method.

Table.1

Statistics of Damages of PZT Transducers

PZT No.	1		2		3		4		5	
Group ID	1	2	1	2	1	2	1	2	1	2
Quality	b	s	b	b	s	b	g	s	g	b
Number of Cracks	8	1	6	6	1	7	-	1	-	6

Group ID: 1 – vertical group of the left side;
2 – vertical group of the right side.

Quality: g – full operability;
s – partial operability;
b – full loss of operability.

Table 1 data give the possibility to estimate the probability of three different events after 60 kilocycles of alternative loading:

1. Saving of full operability of PZT.....0.2.
2. Saving of partial operability of PZT.....0.3.
3. Full loss of operability of PZT.....0.5.

Some patterns of crack location are observed, considering the position of the sensor:

1. Fatigue cracks occur strongly in the cross-sections of PZT that are perpendicular to the direction of the tensile load.
2. Along the length of a transducer, the fatigue cracks distribution is approximately even.
3. There is a relatively weak trend of predominant concentration of fatigue cracks in the extreme transducers of vertical groups (Nos. 1 and 5): 21 cracks of 36.

2.3. Investigation of stress state of transducers embedded in the thin-walled structure

The measurement unit of the ultrasound system of SHM contains two principal components: PZT and its supporting member, which in this paper is presented by the glue layer. The analysis of the stress state of the measurement unit is needed for a more detailed estimation of conditions of destruction at the operation loading. The geometrical sizes of the PZT transducer correspond to the PIC151 that is used in all tests of this paper, and the thickness of the Hysol930.3NA glue layer is accepted to equal 0.25 mm. The Al2024-T3 sheet with sizes 1.15 mm × 80 mm × 240 mm presents the host structure for three collinear transducers with a gap of 1 mm between them (Fig. 2.2). In Fig. 2.2 two options of static loading by uniformly distributed stress of 150 MPa are showed. The mechanical properties of all materials of the model are shown in Table 2.

Table. 2

Material Elastic Properties and Tensile Strength

Material	E , MPa	Poisson's ratio	Tensile strength, MPa
Al2024-T3	71000	0.33	
PIC 151	67000	0.34	~45
Hysol930.3NA	2232	0.42	31

Finite element analysis was executed by using the COMSOL Multiphysics software of the study option Stationary. Because there is double axial symmetry of the model in the coordinate plane xz, the outcome of stress analysis is presented below for one-quarter part of the model. In Fig. 2.3, the general view of the distribution of stresses (in the form of Von Mize's equivalent stress) and deformed shape of the model at tensile longitudinal load are illustrated (Fig. 2.4). It can be seen that the presence of transducers causes a non-homogenous stress state of them and the sheet. Obviously, the mean direct stress of the transducer is always smaller than the one of the sheets, and the difference between these stresses is the monotonically decreasing function of the relative thickness of a sheet. It can also be seen that there is more stress at the boundary of the transducer and the glue layer than at the free external boundary. It means that if the brittle or fatigue failure of the transducer is in a similar type of structure, the destruction of the transducer should start at the internal boundary.

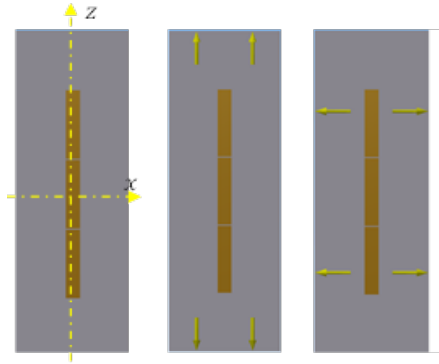


Fig. 2.3. The model of a sample for finite element analysis (FEA) of transducers at two options of loading: tension in the longitudinal and lateral direction.

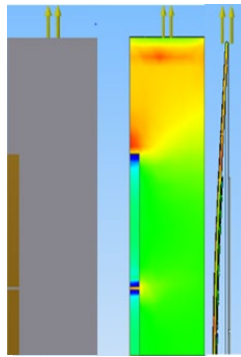


Fig. 2.4. General view of the stress state of the model

For this critical boundary plane, more detailed info on the stress state of the transducer is given in Fig. 2.5. Curves in the interval of coordinate $z \in [0...25 \text{ mm}]$ correspond to half of the middle transducer, and curves of $z \in [26...76 \text{ mm}]$ correspond to the outside transducer. A simple estimation of these outcomes shows that practically in all points of the considered intervals (excluding short-end zones), the acting stresses exceed the tensile (and bending) strength of piezoceramics. It means that at the established level of external loading of sample, at least initiation of brittle cracks in transducers is very probable.

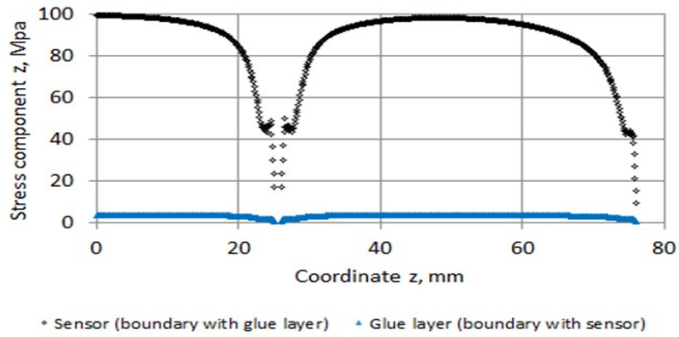


Fig. 2.5. Distribution of tensile stresses of transducers and the glue layer in the boundary plane between them.

A similar analysis was also done for the sample loading in the direction perpendicular to its longest side (Fig. 2.6). Here, the general view of the distribution of stresses (in the form of the Von Mize's equivalent stress) and deformed shape of the model at tensile load are illustrated. The presence of transducers causes a non-homogenous stress state for them and the sheet. The mean direct stress of the transducer is always smaller than the one of the sheets, and the difference between these stresses is the monotonically decreasing function of the relative thickness of a sheet. But in contrast with the previously considered case of tension, Fig. 2.6 demonstrates much less stress in transducers at the same intensity of external loading. Here critical for the strength of the transducer is also the same boundary plane between the transducer and glue layer.

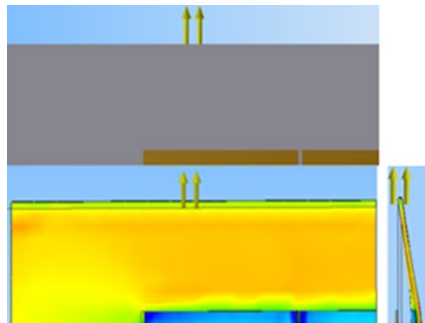


Fig. 2.6 General view of the stress state of the model in tension.

More detailed info on the stress state of the transducer in this plane is given in Fig. 2.7. One specific feature of direct stress distribution is the stress concentration at the end parts of the transducer, and the biggest concentration corresponds to the outside position of the transducer.

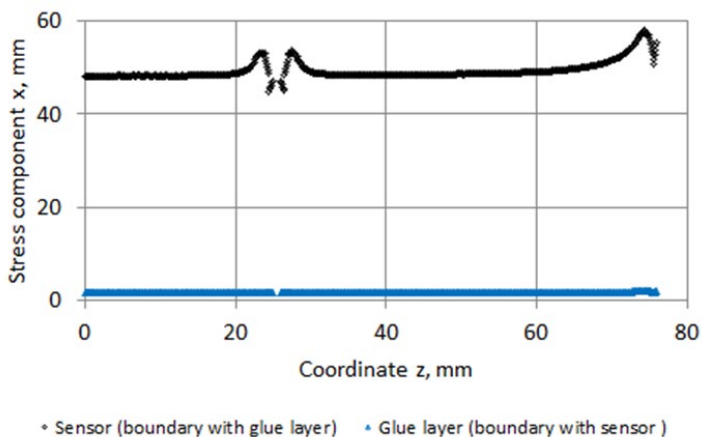


Fig. 2.7 More detailed view of the distribution of tensile stresses of transducers and glue layer in the boundary plane between them.

The information on performed investigation, which is the most important for further use in this paper or for other applications, is given in Table 3. Here the maximum of direct stress parallel to the direction of the tensile load is presented for all boundary planes of each component of the model. The strength of all actual materials also is given in the table, and that allows for estimating the correspondence of any option of transducer installation to the static strength requirement.

Table. 3

Maximum Direct Stress in Boundary Planes of Measurement Unit

Component, its layer	Load direction		Strength, MPa
	longitudinally	transversely	
Sensor, upper free surface	75.03	24.66	45 (80)
Sensor, boundary with glue layer	98.22	58.12	45 (80)
Glue layer, boundary with sensor	3.29	1.94	31
Glue layer, boundary with skin	10.25	3.07	31
Skin, boundary with glue layer	306.31	91.71	350*

In this table, the colour of the cell indicates the status of the static strength requirement: green – requirement is satisfied; yellow – partly satisfied; red – not satisfied.

CHAPTER 3.

ACTIVE METHODS OF SHM USING ULTRASOUND TECHNIQUES

3.1. Electromechanical impedance as primary method of crack detection and load monitoring

3.1.1. Electromechanical impedance, its components, and EMI parameters

The technology of electromechanical impedance (EMI) is selected for the primary detection of fatigue cracks in the skin of the hermetic fuselage. This technology is simple, reliable, and can be effectively realised by using low-cost and simple measurement equipment. In this paragraph, the novel approach to EMI application is considered. It includes the selection of the index of damage (IOD), the definition of its critical value, and the estimation of damage detection using PZT current information only. For the solution of the mentioned problems, the EMI model and results of special tests are used.

Many EMI models have been developed [8]–[17]. A new type of the EMI model and its application for aircraft structural health monitoring (SHM) was developed in [18]. The researcher obtained an expression of the electromechanical impedance common to any dimension of models (1D, 2D, 3D) and directly independent from imposed constraints. The modal analysis of the system “host structure – PZT” dynamic response is the basic tool of this model. The final EMI equation is (Eqs. (1), (2), and (3)):

$$Z(\omega) = \frac{1}{i\omega C} \left[1 + \frac{k_{31}^2 \omega^2}{\left((1 - \nu) - 2 \frac{E'}{E} \nu'^2 \right) Ah} \Phi(\omega) \right]^{-1}, \quad (1)$$

where

$$\Phi(\omega) = \sum_{k=1}^{\infty} \frac{\int f(\xi) dW \int \rho(\xi) (\xi - \xi_c) U_k(\xi) dW}{M_k (\omega_k^2 - \omega^2)} \quad (2)$$

and

$$f(\xi) = (\epsilon_{1k} + \epsilon_{2k} + 2\nu' \epsilon_{3k}) + \frac{d_{33}}{d_{31}} \left(\nu' (\epsilon_{1k} + \epsilon_{2k}) + \frac{E'}{E} (1 - \nu) \epsilon_{3k} \right), \quad (3)$$

where

$k_{31}^2 = d_{31}^2 / (\epsilon_{33} s_{11})$ – the electromechanical coupling coefficient;

s_{11} – the component of mechanical compliance at zero field;

ϵ_{33} – the dielectric constant at zero stress;

d_{31} – the induced strain coefficient, i.e., mechanical strain per unit of electric field;

E and E' – the elasticity modulus;

ν and ν' – Poisson’s ratios of transverse isotropic material of PZT;

$C = \epsilon_{33} A / h$ – the capacitance;

A and h – the electrode area and the thickness of PZT;

$$\epsilon_{jk} = \frac{\partial U_{jk}}{\partial x_j};$$

$$(j = 1, 2, 3);$$

$U_k(\mathbf{x})$ and ω_k – k -th mode shape and frequency.

We can see that this model directly uses the results of modal analysis of the structure and is independent from the details of structure configuration, the boundary conditions, and the external loading. It is the main advantage of this EMI model. In this research, the modal analysis is performed in COMSOL Multiphysics, and its results are transmitted to MATLAB, in which the algorithm of the EMI model is realised.

Further the model of 240 mm × 80 mm × 1.15 mm Al alloy sheet equipped with two sensors PIC151 is shown (Fig. 3.1), used for EMI simulation and for defining the relationship between the EMI index and a crack size in the symmetry plane. The results of simulation give information for a comparative estimation of different types of damage index, and for establishing the reliable procedure of index value determination.

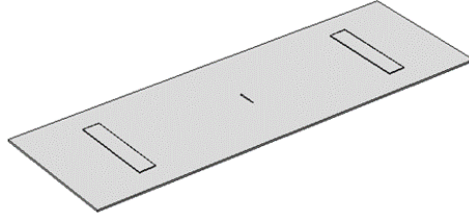


Fig. 3.1 The plate with a crack is equipped with two PZT transducers.

The two types of integral DI were considered here and information was obtained for the comparable estimation: root mean square deviation (RMSD) and correlation coefficient deviation (CCD).

The RMSD index is defined by the following equation:

$$RMSD = \sqrt{\frac{\sum_{k=1}^N [y(\omega_k) - y_0(\omega_k)]^2}{\sum_{k=1}^N [y_0(\omega_k)]^2}}, \quad (4)$$

where y is the current realisation of some signature of EMI, changes of which should be estimated, $y_0(\omega_k)$ denotes the EMI signature in the initial (unloaded) state, and N is the number of sample points in the frequency band of interest (Eq. (4)).

The CCD index is defined by the following equation:

$$CCD = 1 - CC = 1 - \frac{Cove(y(\omega), y_0(\omega))}{\sigma_y \sigma_{y_0}}, \quad (5)$$

where CC is the correlation coefficient that indicates the statistical relationship between two signals: $y(\omega)$ and $y_0(\omega)$ of the EMI signature (Eq. (5)).

The simulation procedure described above was done for all six signatures of the EMI (magnitude of EMI, resistance, reactance, magnitude of EM admittance, conductance, and

susceptance). But the essential features of all these signatures such as reaction to damage are similar. Therefore, those features are illustrated below for some separate signature (Figs. 3.2–3.4). The graphs in these figures show the results of simulation in the frequency band 4–300 kHz with a step of discretisation 100 Hz. DI was calculated in the window of 2000 samples, which corresponds to the width of the window in the frequency domain of 200 kHz. So, in Figs. 3.2–3.4, the frequency corresponds to the initial point of the selecting window, and the ordinate shows the value of DI in this window.

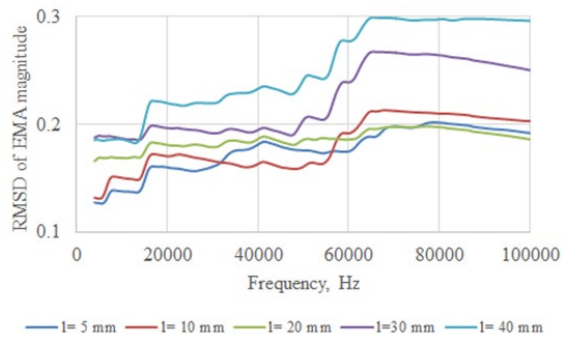


Fig. 3.2. The RMSD of EMI magnitude as a function of the initial frequency of the selecting window.

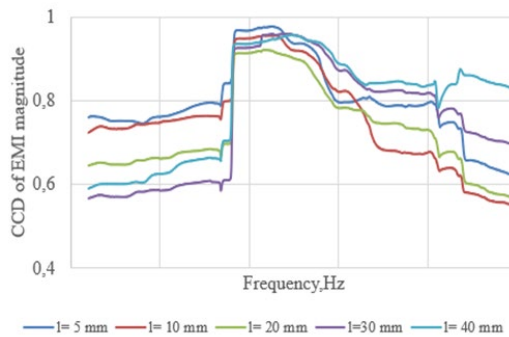


Fig. 3.3. The CCD of EMI magnitude as a function of the initial frequency of the selecting window.

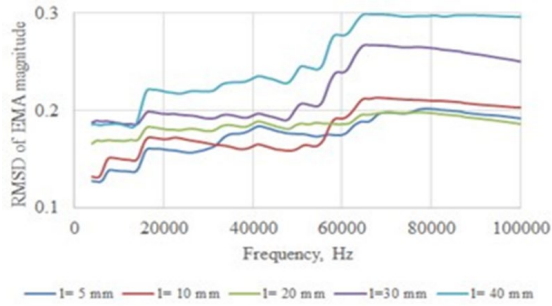


Fig. 3.4. The RMSD of EMA magnitude as a function of the initial frequency of the selecting window.

3.2. Other indices of the electromechanical impedance-based system of SHM

The effect of damage usually is estimated by the index of damage (DI), like RMSD, CCD and other less popular ones. All those indices are integral, but discrete records of the EMI curve cause many local sampling problems. The selection of the width of the window of a data set, the number of sample points, and the frequency band are important for the stability of damage indices. The rational procedure of the EMI damage indices defining is proposed.

There are other indices of EMI in the impedance-based system of SHM. Only one of them is used here as an average or mean value of the EMI signature in the selected frequency band. This index is effective for estimation of the vertical shift of the EMI curve in the frequency domain.

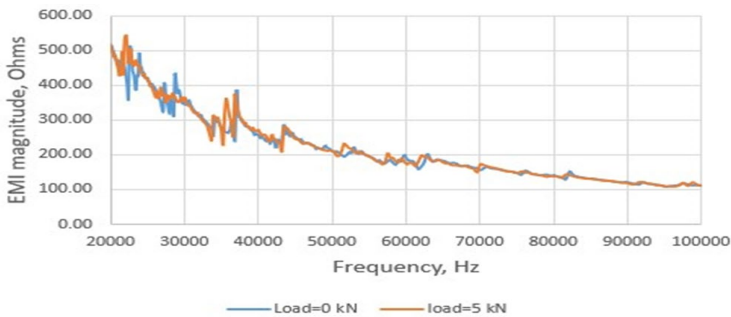


Fig. 3.5. The effect of loading on the spectrogram of EMI magnitude.

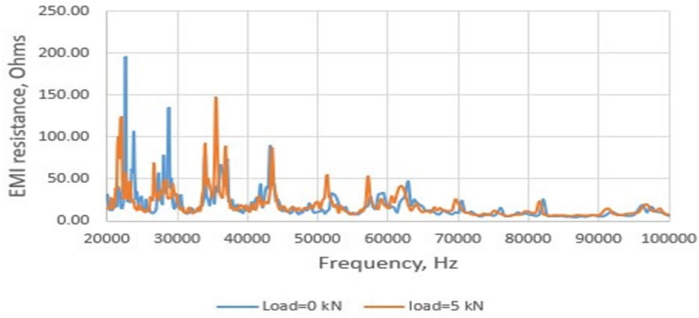


Fig. 3.6. The effect of loading on the spectrogram of EMI resistance.

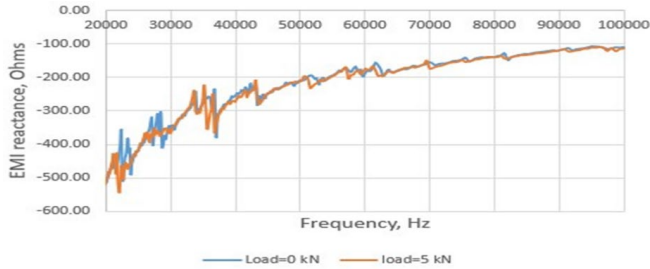


Fig. 3.7. The effect of loading on the spectrogram of EMI reactance.

The data derived from the Cypher Graph is used for the calculations. The effect of load on the electromechanical impedance is determined by plotting different graphs between the loads and the root mean square deviation (RMSD) of EMI. In each graph, the RMSD values of different signatures are plotted against the load. The graphs are obtained for different iterations. The test sample was subjected to periodic loading and unloading. RMSD values always begin from zero.

The graph in Figs. 3.5–3.7 has been obtained between the root mean square deviation of resistance against the load. It is subjected to 6 different iterations, and it shows considerable deviation in the resistance signature. All these readings are obtained from the sensors attached to the sample plate.

3.3. Experimental study of the crack open/close effect and the perspective of its use in structural health monitoring

3.3.1. The aim of experimental investigation

The aim of the experimental study is a more detailed investigation of features of the crack

open/close effect, the comparison of efficiency of different kinds of the damage index and, finally, estimation of real perspective of the creation of a SHM system based on the mentioned effect.

3.4. The test sample, equipment, and setup

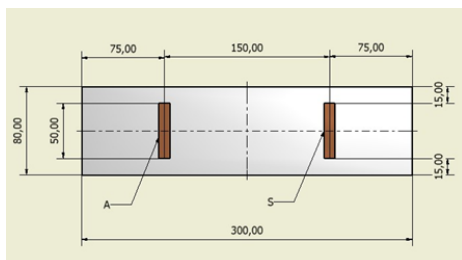


Fig. 3.8. The sample for the fatigue test.

The test sample is an Al2024-T3 sheet, 300 mm × 10 mm × 1.15 mm, with the central hole 4 mm. Two transducers PIC 151 and 0.5 mm × 10 mm × 50 mm (PI Piezoceramic) are connected to the sample by Epoxy Paste HYSOL EA 9309. 3NA QT SYSTEM (the general view of the sample is shown in Fig. 3.8. The scheme of transducers installation is shown in Fig. 3.8. The fatigue test was performed using the Instron 8800 test machine at a cyclic load of maximum 12 kN and minimum 4 kN, and a frequency of 10 Hz. At the stage of crack initiation after each 20 kilocycles, and at the stage of fatigue crack propagation, the loading was interrupted for ultrasonic measurement.

The following measurements were done:

1. The sensor response to specific excitation impulse (five sine waves of frequency 250 kHz modulated by the Gauss error function).
2. EMI of the system “transducer/sample”. Measurements were performed for unloaded and statically loaded states.

The measurement equipment included:

- a. Lamb wave electronics LWDS45 (Cedrat Technology) for generation of excitation impulse.
- b. Software for LWDS45 (KUL) coupled with LWDS45 hardware.
- c. USB450-25: 4 Ch Oscilloscope 25 MHz version (Acquitek) for sensor response measurement.
- d. Impedance measurement C60 (Cypher Instruments Ltd).

3.5. Essential outcomes

In Fig. 3.9 the result of the research in respect of the EMI is shown. The RMSD index of conductance is used here. For other components of EMI, the response is similar.

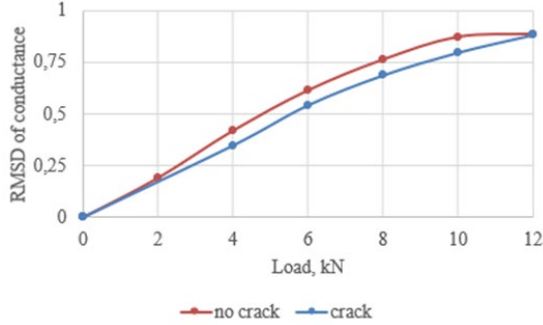


Fig. 3.9. The effect of loading on the conductance of the system.

The novel kind of damage index (DI) is used here for the detection of crack size by using the guided wave technology. Very briefly the essence of DI is explained below. If the function $f(t)$ is the signal that is induced by the excitation impulse $\varphi(t)$ at the crack length l (Eq. (6)), then the integral transform is the convolution of these two functions.

$$\Phi(\tau, l) = \left| \int_0^{\infty} f(t)\varphi(t - \tau) dt \right|, \quad (6)$$

where τ is the shifting variable with a unit of time. The first global maximum of $\Phi(\tau)$ is selected as a measure of damage. It can be obtained by the construction of the left-upper envelope $E(\tau, l)$ of the signal transform $\Phi(\tau, l)$ as follows (Eq. (7)):

$$E(x, l) = \max[\Phi(x, l)], \quad \text{for } x \in [0, \tau]. \quad (7)$$

The value of variable $\tau_c \in [0, \tau)$ that corresponds to the mentioned maximum can be accepted as the time-of-flight. The $E(\tau, l)$ corresponds to the first global maximum of signal transform.

The procedure of $E(\tau, l)$ determination for crack length $l = 13$ mm is showed in Fig. 3.10.

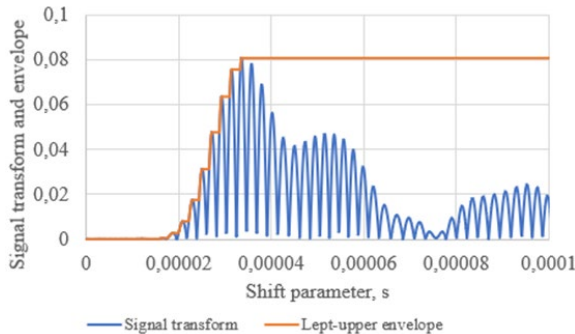


Fig. 3.10. Signal convolutions transform and DI determination.

The dimensionless damage index $DI(l)$ is defined by Eq. (8):

$$DI(l) = 1 - \frac{E(\tau, l)}{E(\tau, 0)}. \quad (8)$$

In Fig. 3.11, the outcome of experimental study is presented. DI is a monotonic function of the crack length. Another important result is the time-of-flight characteristics (Fig. 3.12).

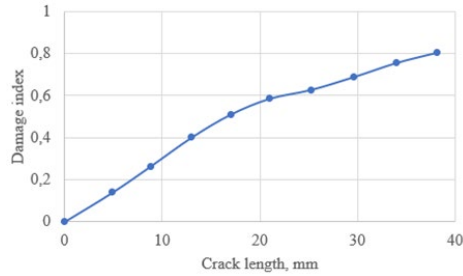


Fig. 3.11. Damage index obtained using the crack length.

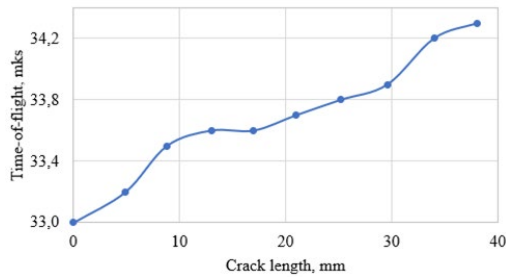


Fig. 3.12. Time-of-flight calculated using the crack length.

3.6. Application of SHM on the skin of hermetic fuselage structure

3.6.1. Demonstration of impedance-based SHM of the hermetic fuselage skin

A small part of typical aeronautical panel of the Al-alloy (2024-T3) hermetic fuselage is taken for the demonstration of previous structural analysis and the definition of basic architecture of its SHM system.

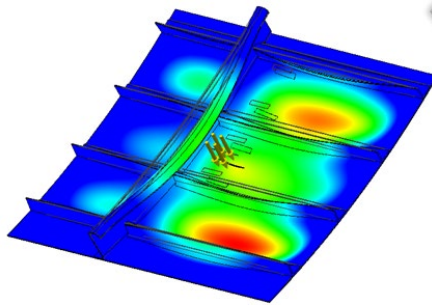


Fig. 3.13. Stress state analysis of a pressured fuselage.

A small part of typical aeronautical panel of the Al-alloy (2024-T3) hermetic fuselage is shown in Fig. 3.13. The direct distance between transducers is equal to 77 mm, the thickness of the skin is equal to 1.5 mm, and the principal curvature radius is equal to 2000 mm. It means that the conditions of problem of the crack detection in the skin are close to the ones considered in the Thesis. The problem of the transducer's own strength can be estimated as well as the expected values of the damage indices for a crack of a given length.

First, stress state simulation of the selected unit of the pressured cabin. Figure 3.13 shows that the maximum stress of the transducer at the boundary with the glue layer is not more than 17 MPa. It means that the requirement of static strength is completely satisfied (see Table 3 in Chapter 2), and probably there will also be no problem of the fatigue strength.

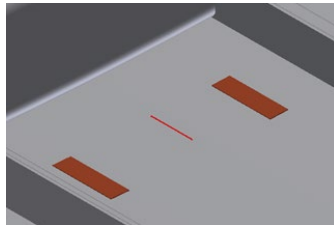


Fig. 3.14. Fragment of a skin with two transducers.

Figure 3.14 presents the fragment of a skin with two PZTs and with a 35 mm crack of between them. These damage indices can be approximately estimated using the results of the above investigation.

EMI in relation to RMSD of EMA magnitude:

non-pressured cabin.....0.285;

pressured cabin.....0.27.

The damage index of guided wave:

non-pressured cabin..... $DI = 0.655$, to $F = 34.2$ mks;

pressured cabin..... $DI = 0.785$, to $F = 35.0$ mks.

3.7. Prediction of fatigue crack growth and estimation of lifetime

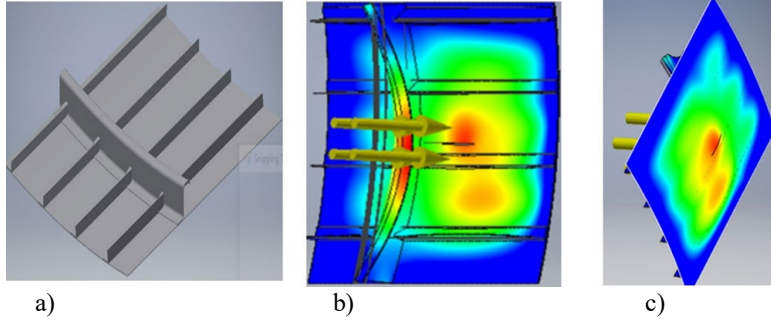


Fig. 3.15. a) Aeronautical panel and b), c) the results of stress state analysis in the presence of a possible fatigue crack.

The geometry modelling is carried out in *Autodesk Inventor*. First, a panel (Fig. 3.15 a) is designed that satisfies the airworthiness requirements. The direct and shear stresses in the skin of fuselage caused by bending and torsion were neglected. It is assumed that in the skin of the panel, circumferential direct stress is two times bigger than the meridional direct stress, and those stresses are caused by air pressure of 100 mPa inside the cabin. So, in the mentioned stress field, the fatigue crack propagates to the longitudinal direction (Fig. 3.15 b) and c)). The stress state analysis is carried out using the *Autodesk Inventor* module *Environments* (option Static Analysis). Two views of full displacements are represented at the same time (Fig. 3.15).

The critical length of the fatigue crack is defined by the condition of crack at the start of growth:

$$K_I = K_{Ic}, \quad (9)$$

where K_I is the stress intensity factor (SIF) that is a crack size function and K_{Ic} is a constant of material, called the fracture toughness (Eq. (9)). It is accepted that

$$K_I = \sigma\sqrt{\pi l} Y(l), \quad (10)$$

where l is a crack half-length, σ is circumferential direct stress in the skin of the panel, $Y(l)$ is the correction multiplier. It can be exactly calculated by using the results of FEA, and is approximately equal to 1 (Eq. (10)).

The mechanical properties of the material of skin define its crack resistance at static and cyclic loading are given in Table 4. C and m are the Paris law constants which describe the crack growth rate at cyclic loading (Eq. (11)).

Using Eqs. 9 and 10 the critical length of the fatigue crack corresponding to the remaining strength of skin 34.6 MPa (circumferential direct stress at maximum pressure in a passenger cabin) is equal to 265 mm.

Table. 4

Mechanical Properties of Al Alloy 2024-T3

Materials	K_{Ic} , MPa \times m ^{0.5}	m	C
2024-T3	26	4.2	8.8×10^{-11}

Prediction of the fatigue crack propagation is done using the Paris law for the rate of fatigue crack growth (Eq. (11)):

$$\frac{dl}{dN} = C(\Delta K_I)^m. \quad (11)$$

It is a simple first-order differential equation. The solution is obtained by a numerical integration at the initial condition: the length of the initial crack is equal to 20 mm. It is a size that can be detected reliably using the EMI method.

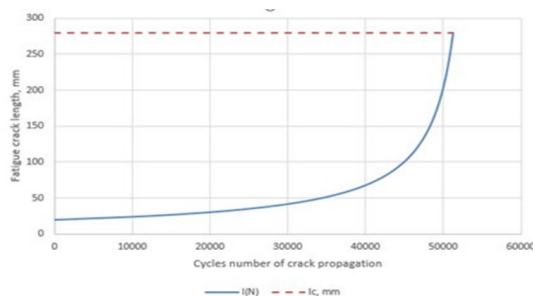


Fig. 3.16. Prediction of the fatigue crack growth and estimation of lifetime.

The result of prediction is shown in Fig. 3.16. It shows that the predicted lifetime of crack propagation to the critical length equals about 50000 flights (Fig. 3.16).

CHAPTER 4. OTHER APPLICATIONS: LOAD MONITORING AND ACOUSTIC EMISSION

4.1. Related application

This chapter discusses other structural monitoring options in which the technical condition assessment is based on current or accumulated information without reference to the initial state. First, this situation is developing if the load and other external influences should be monitored. The intensity of the mechanical load, its variable nature, dynamic effects, temperature effects, corrosion damage and other effects of the concomitant influence of the environment are the main factors that determine the degradation of the structure during operation. If the influence of each of these factors and their mutual influence on the lifetime of the structure are measured and properly considered, then on this basis, it is possible to build a built-in monitoring system that is able in a statistical sense to predict the degree of damage and to assess the degree of danger of approaching a critical state. Such a comprehensive system for monitoring external influences would allow a more accurate assessment of their cumulative effect but would be cumbersome and expensive to produce and operate. Therefore, in practice, to ensure the optimal combination of forecast accuracy and economic efficiency, they are limited only to measuring the parameters that have the greatest impact on the lifetime of the structure in operation. In many cases, the load is the determining parameter. In particular, the mechanical load is the main external influence that determines the fatigue life of the components of the main structure of aircraft made of metallic

materials. On the principle of monitoring the external load and assessing its cumulative effect, a monitoring system for the main structure and power units of modern helicopters has been built [19], [20], demonstrating high efficiency in operation.

Load monitoring involves an indirect way to assess the structural health of a structure. This estimate can be obtained using an acceptable generalised damage parameter determined by the results of load monitoring and its comparison with the strength characteristics of the controlled structural element. The fundamental problems of implementing this approach in relation to fatigue damage to a metal structure are discussed in Section 4.2. Both compared quantities are random. Therefore, the damage index should have a probabilistic formulation and be perceived as a requirement for additional verification and assessment of the technical condition of the structural element in question. The procedure of this type is developed in [21], and its fundamental fragment is presented in Section 4.3.

A similar use case for the passive response of a piezoelectric transducer provides acoustic emission monitoring. It can be effectively used in endurance fatigue tests [22] and is described in Section 4.4.

4.2. Load monitoring using PZT response

One of the most important studies related to load such as axial, transverse, and fatigue are the main sources of structural damage. Thus, this article presents the behaviour of EMI technology for structural load monitoring (SLM), which is a part of SHM [23].

In Section 6.5, the requirements for fatigue testing of full-scale bench test are determined in order to define the service life of aircraft structures, which have direct influence on flight safety. The research focus is on the solutions for how to extend the total service life of parts which have limited-service life. To reasonably extend the resource of limiting elements, close to real data are presented about loading of these elements during the regular flight mode, as well as data of real scale model testing and strength analysis. Using this data, evaluation of short time strength and durability of parts can be achieved.[24]

4.2.1. Stress and load measurements

Below, three approaches are considered to load (stress) measurement by transforming the mechanical parameter to proportional electrical response.

The effect of mechanical tension to electrical resistance of the conductor caused by changing of geometrical sizes without changing material properties is strain gauge.

The change of electrical resistance of metallic wire at its tension was reported in [19]. This phenomenon was investigated for a large number of materials [20] in a wide range of strain. The dynamic technique of electrical resistance measurement was presented in [21].

1. There was established and embedded in practice linear relation between elastic strain ε and the relative resistance of strain gauge $\Delta R/R$.

$$\frac{\Delta R}{R} = GF \cdot \varepsilon, \quad (12)$$

where GF is a constant, which is called the gauge factor.

In the case of metal, the total change of resistance is caused by the geometry changes of wire: length l and cross-section area A (Eq. (13)):

$$R = \rho \frac{l}{A}, \quad (13)$$

where ρ is specific resistance (resistivity) of material.

2. The piezo resistance effect.

The term piezo resistance was first used in [25]. For semiconductors, the resistivity is not constant but also changes at loading, as shown in [26].

$$\frac{\Delta R}{R} = \frac{\Delta \rho}{\rho} + (1 + 2\mu)\epsilon, \quad (14)$$

where μ is the Poisson's ratio.

For linear strain, the relation (Eq. (12)) remains the same, but its value is more than 50 times larger than the metallic strain gauge (Eq. (14)).

The tensor theory of piezo resistance was developed in [27], and all recent year's achievements are described in [28].

3. Piezoelectricity effect.

The interaction between the electrical and mechanical variables of linear piezoelectric materials can be described by a constitutive relation in the tensorial form. Below, there are presented so-called sensing piezoelectrical equations in compressed form (Eq. (15)):

$$\begin{cases} \{\mathbf{S}\} = [\mathbf{s}] \{\mathbf{T}\} + [\mathbf{g}] \{\mathbf{D}\} + \{\boldsymbol{\alpha}\} \theta \\ \{\mathbf{E}\} = [\mathbf{g}]^t \{\mathbf{T}\} + [\boldsymbol{\beta}] \{\mathbf{D}\} + \{\mathbf{B}\} \theta \end{cases} \quad (15)$$

where

$\{\mathbf{S}\}$ – the strain vector which presents strain tensor in compressive form;

$[\mathbf{s}]$ – the compliance matrix;

$\{\mathbf{T}\}$ – the stress vector which presents stress tensor in compressive form;

$[\mathbf{g}]$ – the matrix of the coupling between the electrical and the mechanical variables;

$\{\mathbf{D}\}$ – the vector of electric displacements;

$\{\boldsymbol{\alpha}\}$ – the vector of coefficients of thermal expansion;

$\{\mathbf{E}\}$ – the vector of electric field;

$[\boldsymbol{\beta}]$ – the vector of impermeability;

$\{\mathbf{B}\}$ – the vector of piezoelectric voltage coefficients;

θ – temperature.

Equations (15) describe linear piezoelectricity and, together with a system of equations for the theory of elasticity, allow to solve the problem of piezoelectricity for any linear piezoelectric device.

Below, several types of piezoelectric devices are considered with respect to their use of them for stress or load measurement.

4.2.2. Homogenous stress state of PZT

For this case, the solution can be easily obtained directly from Eq. (15) using the properties of PZT constants of material. But, here and anywhere in this section, the solutions are obtained in a numerical way using *COMSOL Multiphysics* software. It allows to save a single style of results presentation and convenience of their comparison. The stationary study of the free sensor at homogenous loading is presented in Table 5. The electrical potential of PZT is a response

which is proportional to load (stress) (Figs. 4.1–4.5).

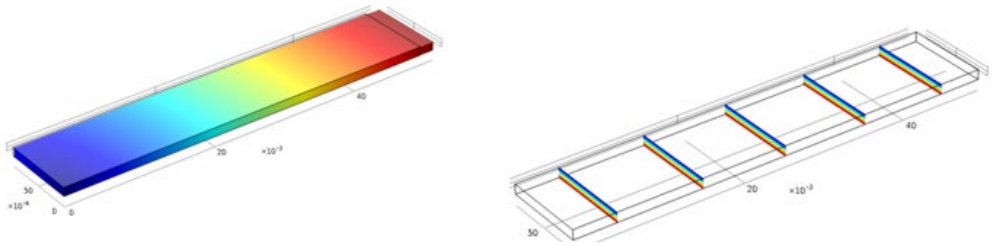


Fig. 4.1. Unidirectional tension in the longitudinal direction of the PZT.

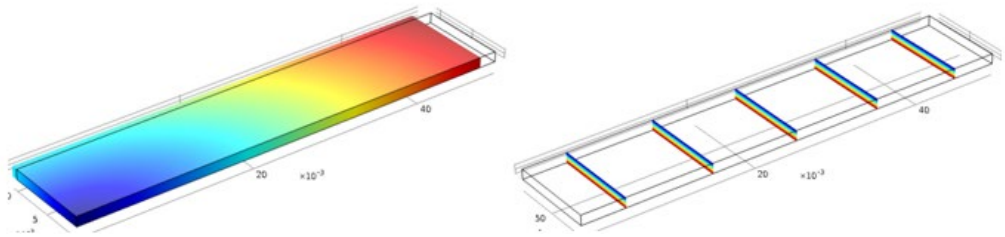


Fig. 4.2. Unidirectional tension in the lateral direction of the PZT.

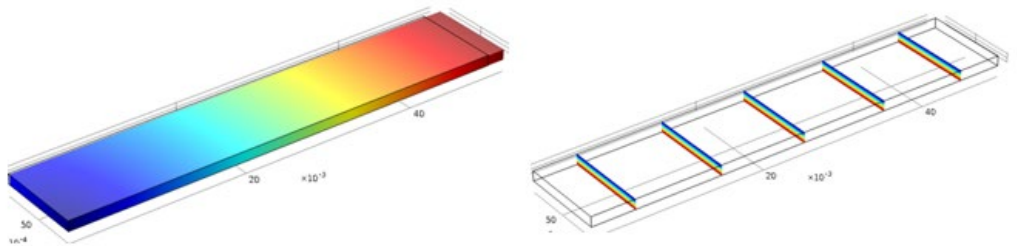


Fig. 4.3. Uniform tension in all directions in a plane.

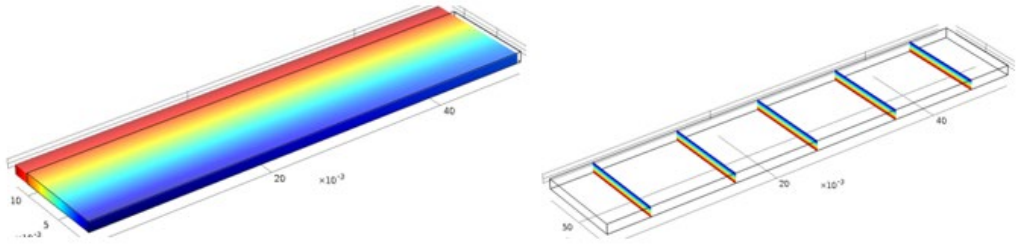


Fig. 4.4. Tension in two perpendicular directions in a plane $S_x = 5$ MPa, $S_y = 10$ MPa.

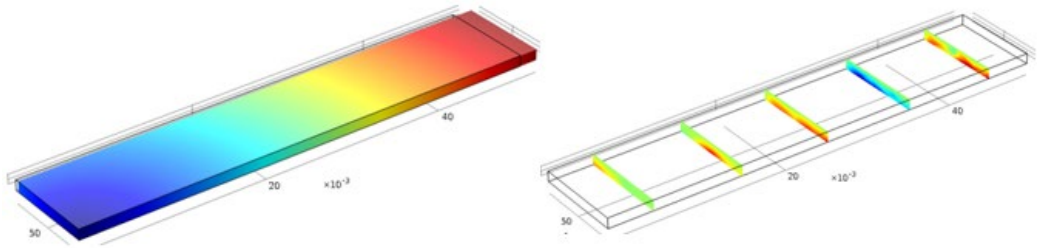


Fig. 4.5. Pure shear (regarding principal stresses $S_x = 5$ MPa, $S_y = -5$ MPa).

Table. 5

Generalised Information on the Homogeneous Stress State of the PZT

Type of plane stress state			Total displacement, mm	Potential, V
σ_x , MPa	σ_y , MPa	τ_{xy} , MPa		
5	0	0	0.0036	65.3
0	5	0	0.0020	65.3
5	-5	0	0.0056	0
5	5	0	0.0017	130.6
5	10	0	0.0006	196.0

4.2.3. Non-homogenous stress state of PZT

The low plane of the sensor is constrained: displacement, which is perpendicular to this plane, is equal to zero ($w = 0$). Loading of the sensor is executed by the uniform tension (compression) of the constraining plane. (Fig 4.6 – 4.9).

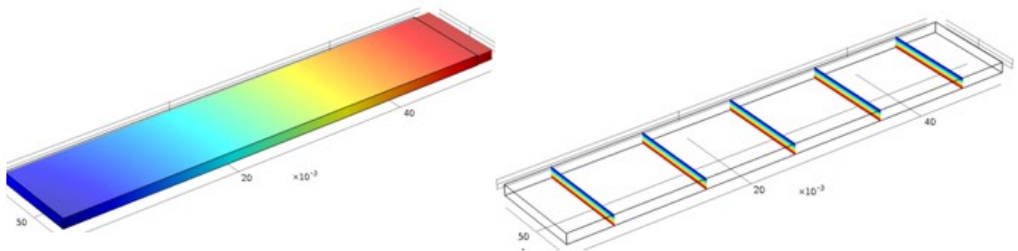


Fig. 4.6. Unidirectional tension of the constraining plate in the longitudinal direction of the PZT.

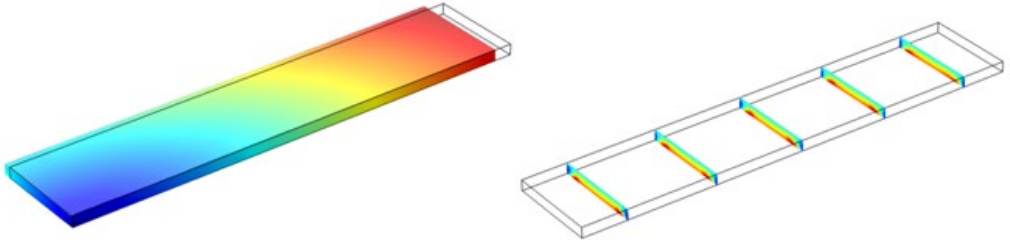


Fig. 4.7. Unidirectional tension of the constraining plane in the lateral direction of the PZT.

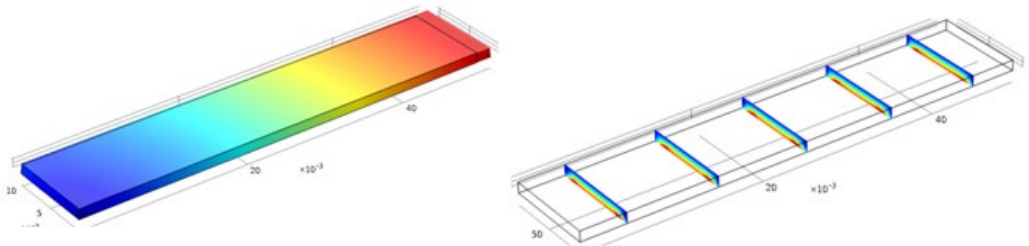


Fig. 4.8. Uniform tension of the constraining plane in all directions in a plane

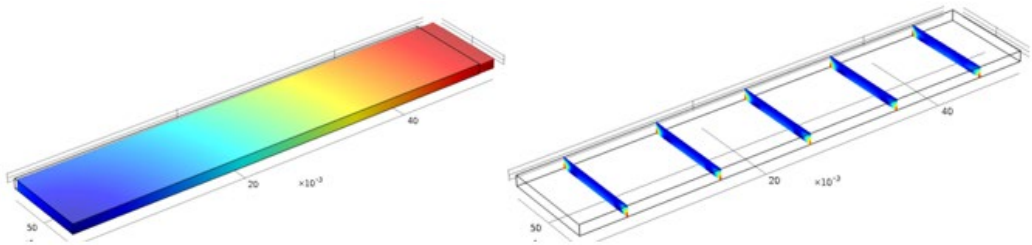


Fig.4.9. Pure shear of the constraining plate (regarding principal stresses).

Table. 6

Effect of the PZT Stress State Type on its Electrical Potential

Type of plane stress state			Potential, V		
σ_x , MPa	σ_y , MPa	τ_{xy} , MPa	Homogeneous stress state	Non-homogeneous stress state	
				Boundaries	Volume
5	0	0	65.3	64.0	65.3
0	5	0	65.3	59.1	65.3
5	-5	0	0	20.7	20.4
5	5	0	130.6	114.6	122.1
5	10	0	196.0	151.7	138.7

4.2.4. The PZT embedded in thin-walled plate

In this section, the effect of load typical transmission to the PZT PIC 151, $0.5 \text{ mm} \times 10 \text{ mm} \times 50 \text{ mm}$ (PI Piezoceramic) is simulated and analysed. The rectangular Al-alloy sheet of $1.15 \text{ mm} \times 80 \text{ mm} \times 150 \text{ mm}$ is equipped with a PZT of $0.5 \text{ mm} \times 10 \text{ mm} \times 80 \text{ mm}$, as is shown in Fig. 4.10. The PZT is attached to the sheet by a 0.25 mm layer of the above-mentioned epoxy paste HYSOL EA 9309. 3NA QT SYSTEM.

Below are presented the results of a simulation for two different loading options on this sample.

1. Imitation of a tension sheet in the test machine.

The upper and bottom edges are clamped, and the direct stress of the tension in the cross-section of a plate is equal to 40 MPa . It can be seen that the presence of PZT causes local bending of the sheet and complex loading of PZT (Fig. 4.10).

The mean (in PZT volume) stress component $\sigma_y = 5.72 \text{ MPa}$.

The mean (in PZT volume) stress component $\sigma_x = -5.05 \text{ MPa}$.

Considering the symmetry of a structure about axis 'x' and 'y', it can be concluded that the stress state of a PZT is close to the pure shear. In this case, as shown above, the electric potential is relatively low and is equal to 3.81 V .

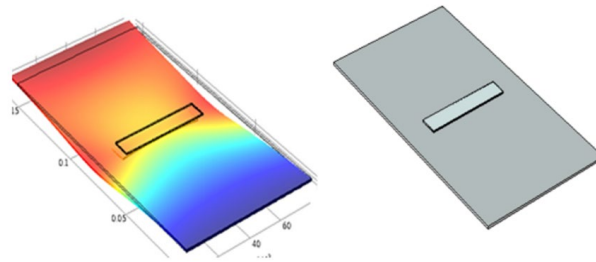


Fig. 4.10. The Al plate with PZT at tension by stress 40 MPa .

2. Two-directional tension. Imitation of in-plane loading of a skin of hermetic fuselage.

The boundary conditions at the outer counter are set in displacements. The total elongation:

in axis x, the direction is equal to 0.0229 mm ;

in axis y direction is equal to 0.0852 mm .

It can be seen that the presence of PZT causes local bending of the sheet, but deflection is significantly less than at unidirectional tension (compare Figs. 4.10 and 4.11).

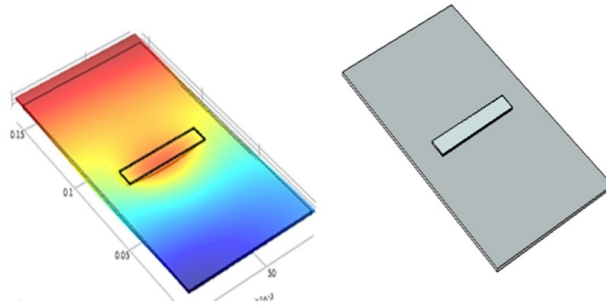


Fig. 4.11. The Al plate with PZT at two-directional tension.

Those displacement boundary conditions correspond to average boundary stresses:

- 1) for horizontal boundaries, the stress component $\sigma_y = 54.7$ MPa;
- 2) for vertical boundaries, the stress component $\sigma_x = 35.5$ MPa.

The complex stress state of PZT is:

- 1) the mean (in PZT volume) stress component $\sigma_y = 6.99$ MPa;
- 2) the mean (in PZT volume) stress component $\sigma_x = 13.8$ MPa.

The electric potential is equal to 117.9 V.

4.3. Equivalent stress and fatigue limit

Load monitoring is relevant for dynamically loaded structures, especially for metallic units of machines and mechanisms. This is caused by the effect of fatigue, which is produced by alternative long-time-acting load and expressed in the fatigue crack initiation. Cracks are one of the most dangerous types of structural damage because they induce progressive, very significant decrease in strength.

Airworthiness requirements allow the fatigue cracks of the bearing components of aircraft in operation (the safe-fail principle) [29]. But, the remaining structural strength cannot be less than an established minimum.

Miner was the first to propose deriving the linear cumulative damage rule [30]. A large number of tests with variable amplitude were carried out to verify Miner's rule, and a detailed overview of the results can be found in [31]. There, it is shown that the total cumulative Miner's sum at failure varies from much smaller than 1 to significantly larger than 1. In [32], the idea of the realistic Miner's rule is discussed, and it is pointed out that improving the prediction of the fatigue lifetime requires test results at load-like operational.

It is known that the Miner's damage count significantly depends on a description of the loading history [31], [33]. The most popular is the so-called rain flow counting method [34]. A similar method was proposed in [35].

4.3.1. The model of structural health assessment using load(stress) monitoring

The passenger aircraft operation process can be considered as some sequence of flights, each of them can be estimated by two general parameters: the working time τ_i of flight number i and intensity of external load, which there is estimated by the fatigue damage of this flight D_i . Both

are random variables. Also, there the assumption that the load of all flights is statistically similar. In Fig. 4.12, the schematic structure of stresses in the skin of a wing panel is shown for two flights i and $i + 1$. The blue line corresponds to the load, which is recorded by the system of SHM. It is demonstrated that there is a difference between both general parameters of two sequential flights.

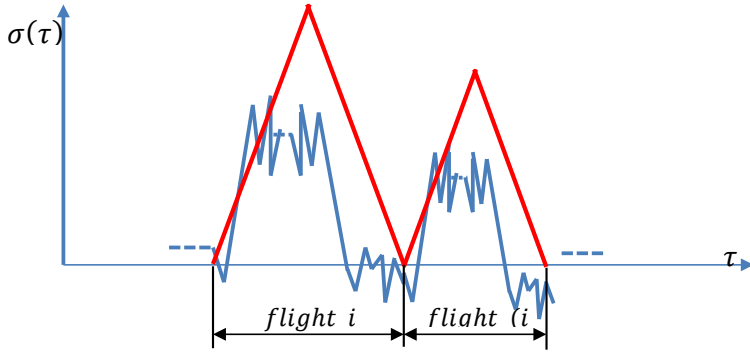


Fig. 4.12. The schematic record of the skin stress by SHM system (blue) and the equivalent cycle of stresses (red).

The Miner's count of separate flight D_i calculated by the rain flow counting method is used to estimate fatigue damage (Eq. (16)).

$$D_i = \sum_{k=1}^m \frac{\tilde{n}_k}{N_f(\sigma_k)}, \quad (16)$$

where

σ_k – the level k of cyclic stress in the spectrum of flight i ;

m – total number of levels of cyclic stresses in the spectrum of flight i ;

\tilde{n}_k – the number of cycles of the k level in the spectrum of flight i ;

$N_f(\sigma_k)$ – the fatigue lifetime of structural component at test with the stress of level k .

Here, it is accepted that for the considered structural component, the full Woehler curve is the function between the number of cycles N_f for the fatigue failure (fatigue lifetime) at action of cyclic load with maximum stress σ_f and stress ratio R (Eq. (17)).

$$F(\sigma_f, R, N_f) = 0 \quad (17)$$

There are several parameters of fatigue curve. For the full curve, there must also be the probability of failure.

For each flight, an equivalent flight can be established: it is a hypothetical flight in which all fatigue damage is produced by one cycle of loading. In Fig. 6.13, the equivalent flights i and $i + 1$ are represented with a red line. The condition of equivalence in fatigue damage is equal in real and equivalent flights (Eq. (18)):

$$D_i = \sum_{k=1}^m \frac{\tilde{n}_k}{N_f(\sigma_k)} = \frac{1}{N_f(\sigma_{ei})}, \quad (18)$$

where σ_{ei} is equivalent stress of flight i .

As a result, the damage index can be established as follows.

1. For current number of flights N , the estimate of average equivalent stress should be calculated (Eq. (19))

$$\bar{\sigma}_e(N) = \frac{1}{N} \sum_{i=1}^N \sigma_{ei} \quad (19)$$

2. For the same N from fatigue life curve, the fatigue resistance stress $\sigma_f(N)$ can be obtained (for example, mathematic expectation $\bar{\sigma}_f(N)$).

3. The convenient shape of damage index is:

$$in(N) = \frac{\bar{\sigma}_e(N)}{\bar{\sigma}_f(N)}. \quad (20)$$

This index increases from 0 (before operation start) till 1 (at full consumption of fatigue life) (Eq. (20)).

If for index calculation, mathematic expectations of comparable parameters are used, then the allowable value of index $[in]$ must be restricted using the reliability coefficient f (Eq. (21)):

$$[in] = \frac{1}{f}. \quad (21)$$

Example 1. Define the fatigue damage index of the structural component as a function of number of flights if the fatigue lifetime curve is described by power function:

$$\sigma_f^\alpha N_f = C, \quad (22)$$

where α and C are parameters of the fatigue lifetime curve of material, σ corresponds to maximum stress in cycle at constant stress ratio $R = 0$. Accept that the average equivalent stress at large number of cycles is stable and equal to 50 MPa. The parameters of the fatigue lifetime curve are $\alpha = 2$ and $C = 5 \cdot 10^5$ (Eq. (22)).

It can be seen that in this simple example:

$$in(N) = \frac{\bar{\sigma}_e(N)}{\left(\frac{C}{N}\right)^{\frac{1}{\alpha}}}. \quad (23)$$

The results of calculation are presented in Fig. 4.13. The allowable value of index $[in]$ is defined using $f = 1.5$ (Eq. (23)).

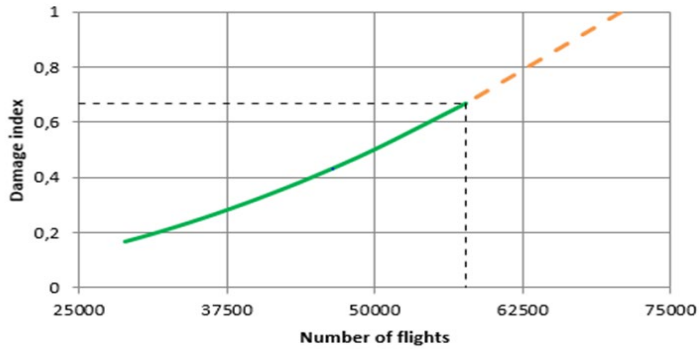


Fig. 4.13. Damage index as the function of number of flights.

The probabilistic approach of construction of fatigue damage index is analysed in [37] and presented in the next section.

4.4. Probabilistic model of strength for SHM of lifetime usage load monitoring

In summary, the SHM framework of a dynamic probability modelling-based aircraft is a powerful tool for predicting the probability of failure or fault in an aircraft. By continuously monitoring the aircraft and analysing the data using statistical modelling and analysis techniques, it is possible to optimise the maintenance schedules and repair efforts, reducing downtime and minimising the risk of accidents or catastrophic failures.

4.4.1. Health and Usage Monitoring System (HUMS)

The data collected through HUM can be used to schedule maintenance and repairs more effectively, allowing for more efficient use of resources and reduced downtime. HUM can also be used to optimise equipment performance by identifying areas where improvements can be made, such as through changes to operational procedures or the use of different materials.

Prognostic health monitoring (PHM) is a method of monitoring the performance and health of a system or equipment in real-time to predict and anticipate potential failures before they occur. It uses a combination of sensors and analytical techniques to collect and analyse data and machine learning algorithms to predict future performance and anticipate potential failures. PHM can be applied to a range of systems and has numerous benefits, including reducing downtime, minimising risk, and optimising maintenance schedules.

Vibration health monitoring (VHM) is a technique used to monitor the health and performance of machines and mechanical systems by analysing the vibration patterns generated by the equipment. By detecting and diagnosing potential faults, VHM can help to perform maintenance and repair activities proactively, reduce downtime, and minimise the risk of catastrophic failures. VHM is widely used in various industries, including manufacturing, transportation, and energy production.

4.4.2. Mathematical model

All random variables associated with the operation of technical systems, as a rule, conform to the normal Gaussian law of distribution (Eq. (24)). Assuming that this is true for the random variables $\Delta\sigma$ and $\delta\sigma$, expressions will be as follows:

$$P_{fa} = \frac{1}{2\pi} \int_{-\infty}^{\sigma_{pv}-m_\sigma} \frac{1}{S_1} e^{-\frac{(\Delta\sigma-m_\sigma)^2}{2S_1^2}} \int_{\sigma_{pv}-m_\sigma-\Delta\sigma}^{+\infty} e^{-\frac{(\delta\sigma)^2}{2S_2^2}} d\delta\sigma d\Delta\sigma; \quad (24)$$

$$P_{pv} = \frac{1}{2\pi} \int_{\sigma_{pv}-m_\sigma}^{+\infty} \frac{1}{S_1} e^{-\frac{(\Delta\sigma-m_\sigma)^2}{2S_1^2}} \int_{-\infty}^{\sigma_{pv}-m_\sigma-\Delta\sigma} \frac{1}{S_2} d\delta\sigma d\Delta\sigma, \quad (25)$$

where S_1 and S_2 represent the mean square deviation of values $\Delta\sigma$ and $\delta\sigma$.

For the convenience of the numerical integration of Eqs. (24) and (25), let us change the variables by analogy with a similar probabilistic task solution described in [36]. Here we will introduce new variables (Eqs. (26) and (27)):

$$y_1 = \frac{\Delta\sigma - m_\sigma}{S_1} \quad \text{And} \quad y_2 = \frac{\delta\sigma}{S_2} \quad (26)$$

$$\text{and designate parameters } c = \frac{\sigma_{pv}-m_\sigma}{S_1}. \quad (27)$$

Then, Expressions (24) and (25) will be as follows:

$$P_{fa} = \frac{1}{2\pi} \int_{-\infty}^c e^{-\frac{y_1^2}{2}} \int_{b-ay_1}^{+\infty} e^{-\frac{y_2^2}{2}} dy_2 dy_1; \quad (28)$$

$$P_{pv} = \frac{1}{2\pi} \int_c^{+\infty} e^{-\frac{y_1^2}{2}} \int_{-\infty}^{b-ay_1} e^{-\frac{y_2^2}{2}} dy_2 dy_1, \quad (29)$$

where $a = S_1 / S_2$, $b = \frac{\sigma_{pv}-m_\sigma}{S_2}$.

The result of solving the system of Equations (28) and (29), obtained by using the well-known numerical methods, is given in Fig. 4.14 in the form of nomograph for the parameters a , b , and c .

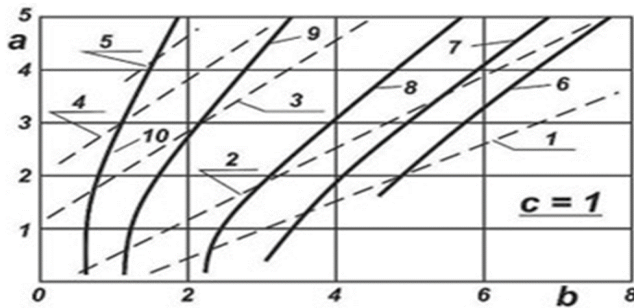


Fig. 4.14. Nomograph for determining the parameters a , b and c .

The probability of omitting a dangerous situation with disastrous effects ($1 - P_{pv} = 1.5 \cdot 10^{-1}$; $2 - P_{pv} = 10^{-1}$; $3 - P_{pv} = 10^{-2}$; $4 - P_{pv} = 10^{-3}$; $5 - P_{pv} = 10^{-4}$).

The probability of the false actuation of the display system

($6 - P_{fa} = 10^{-4}$; $7 - P_{fa} = 10^{-3}$; $8 - P_{fa} = 10^{-2}$; $9 - P_{fa} = 10^{-1}$; $10 - P_{fa} = 2 \cdot 10^{-1}$).

As we can see from (Fig. 4.14), at the given probabilities P_{fa} and P_{pv} , as well as at the parameters of the distributions of the random variables m_{σ} , S_1 , and S_2 , and at the given value σ_{pv} , the value of the limit parameter σ_{pv}^1 can be determined.

4.5. Acoustic emission

One advantage of acoustic emission (AE) over other ultrasonic methods is that it is a passive method, meaning it does not require an external energy source to be applied to the material being monitored. This makes it a useful method for continuous monitoring of structures over long periods of time, as there is no risk of introducing further damage to the structure due to the monitoring process.

However, one potential limitation of AE is that it can be difficult to distinguish between different types of damage based on the frequency range of the stress waves detected. Additionally, interpretation of the data collected by AE sensors can be complex and requires skilled analysts to accurately identify and classify different types of damage.

This chapter intends to present recent trends and applications of AE as passive methods for damage detection technique for helicopter structures [37].

One of the most important exploitation criteria related to helicopter's structure is the service life. The structure consists of elements with limited-service life. These elements have a direct influence on flight safety. For example, these elements are some separate structural elements of planer, blades and joints of main rotor, tail rotor, main gear-reducer, sub-reducer, tail reducer, main and tail shafts, etc. [24].

The only solution how to extend the total service life of a helicopter is a rapid extension of the service life of those elements which have limited service life till they match the value of the helicopter planar service life value. To reasonably extend the resource of limiting elements (elements which set the limits), close to real data must be presented about the loading of these elements during the regular flight mode, as well as data of real scale model testing, strength analysis, etc. Nowadays, there is a limited selection of such materials, so it is necessary to perform real full-scale testing in laboratory/stand to identify the service life values of structural elements in flight mode. The obtained data should be used in additional (double check) calculation of the service life of the parts of structural elements of the helicopter. These calculations must be aimed at evaluation of short time strength and durability of parts. As a result, a final report must be prepared with conclusions about reasonable extension of service life.

The aim of the fatigue testing is to choose the method for fastening mid and tail reducers in precise position, and the same is applied for planer construction (tail beam and fin), placing the reducers according to the fatigue requirements [24].

According to the results of testing, the following actions must be taken:

- The value of technical lifetime should be stated (period of lifetime when it is possible to operate the planer of helicopter due to economic considerations).
- The period of operation till the first maintenance/observation must be stated.
- The duration of maintenance work must be defined to operate helicopter safely.
- The proper parameters of exploitation loads must be defined (ability to withstand loadings within period, with some fatigue cracks in construction) [24].

However, the solutions of all the above tasks are not possible only by “stand” testing of isolated parts (reducers, engine etc.) because such tests do not consider the influence of “neighbouring” parts. The planer constructions must be loaded in such a way that each zone is subjected to the indicated load. The fatigue testing is being carried out on the helicopter’s planer (Fig. 4.15) [24].

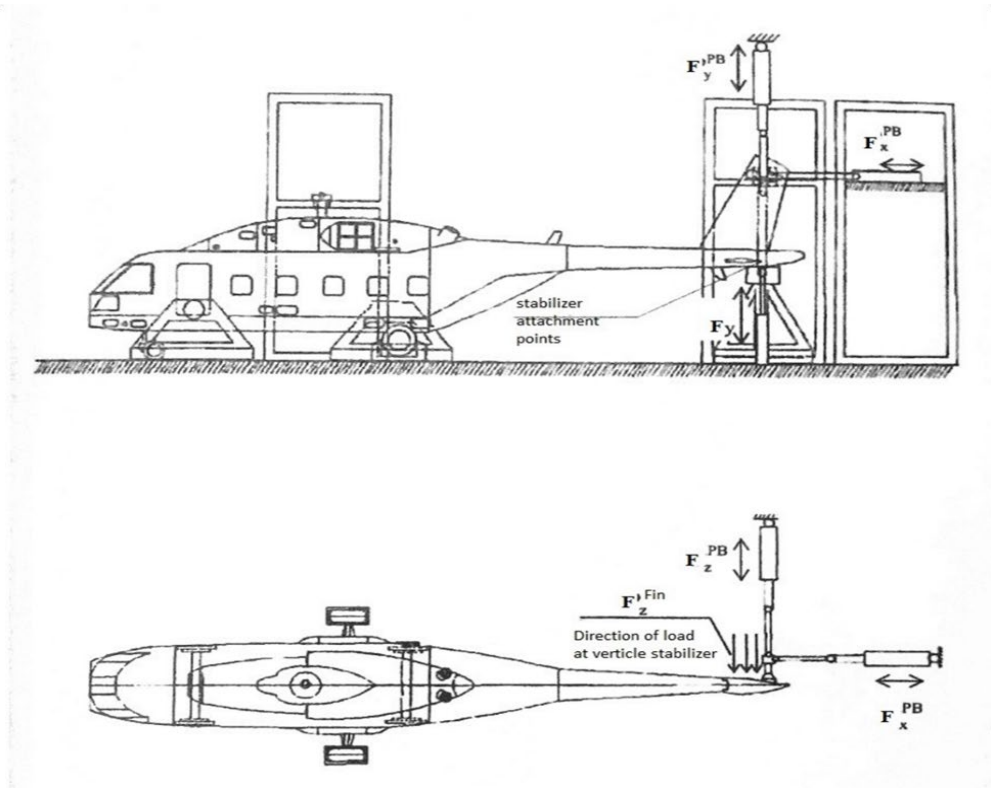


Fig. 4.15. A model of experimental stand for testing the fatigue life of the tail beam and vertical stabiliser of the helicopter [24].

The co-ordinate system used in this experiment is shown in Fig. 4.16.

The X axis is aligned to the flying direction (it is in the middle of the fuselage).

The Y axis is perpendicular to the X axis and is oriented up.

X and Y axis are in the middle of the fuselage (narrow plane).

The Z axis is perpendicular to the XY plane.

Zero point of the coordinate system is located on the X axis, where it is being crossed by the power frame.

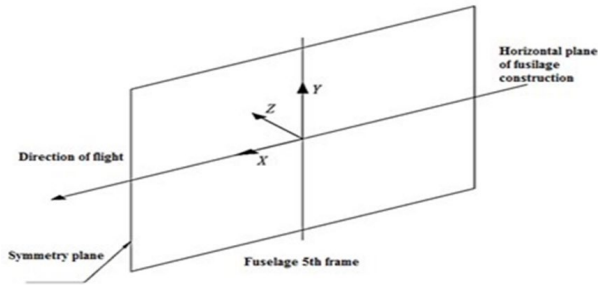


Fig. 4.16. Defined system of co-ordinates [24].

All measuring equipment must be certified and must have a precise rate. This equipment must not exceed $\pm 5\%$ error in measurements.

The laboratory is responsible for selecting the type of deformation sensors. The error measurement for deformation sensors must not exceed $\pm 5\%$ of the maximum value of tension [24].

Requirements for the testing stand.

The testing stand must have all necessary equipment which provide the possibility to do testing if the planer is fixed in one of the following ways:

- a) [on power floor] structural chassis frame is being used;
- b) the planer is fixed by the tail rotor shaft, landing gears do not touch the ground [38];

The stand equipment must be able to apply static load (Fig. 4.15):

- a) to tail rotor at points FPB_x , FPB_y , FPB_z ;
- b) to the joint point of fin;
- c) to spread load F fin z , which is applied to fin [24].

The stand must be equipped with a system which allows rapid control of applied loads and automatic registration of results.

4.6. Some results for full scale test of passive SHM system by using acoustic emission

As an illustration of using integrated piezoelectric sensors to monitor the structure during bench tests, an example of planning and conducting fatigue tests of a full-size component of a light helicopter structure is given below, in which the Thesis author took active part. The main task of the tests was to experimentally demonstrate the fatigue durability of the most loaded (ceiling) part of the frame of the helicopter body with an equivalent bench loading. To control the technical condition of the tested structure, it was envisaged to use the method of acoustic emission, as a passive method of ultrasound diagnostics.

4.6.1. Brief information about the installation of piezo converters acoustic emission

In the process of conducting fatigue tests of the right ceiling part of frame No. 4 of the helicopter, an 8-channel Vallen AMSY-6 system was used. The registration of AE signals was carried out through seven channels (2–8 AE sensors). AE sensors were installed in the application

area of a cyclic load according to the terms of reference (Fig. 4.17).

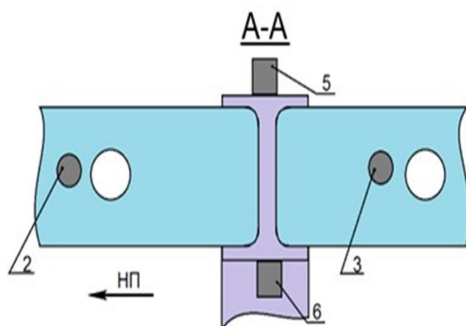


Fig. 4.17. Location and numbering of acoustic emission sensors on the right ceiling side of the frame No. 4 (2–8 AE sensors).

During the fatigue test signal amplitude, energy, total score, signal duration, signal rise time, voltage at the parametric input, threshold value, signal strength, and average signal strength was recorded.

4.6.2. Additional test modes during AE control and presentation of some results

The main criterion characterising the formation and development of fatigue cracks is the change in the total account for each registration channel. In addition to the current control of changes in the specified AE parameters in each loading cycle, to increase the reliability of the control, measurements of the AE parameters were made under static loading according to the following program: periodically every 500 thousand cycles. The loading cycles produced a stepped static loading with shutter speed shelves of 4 minutes according to a special program (Fig. 4.18).

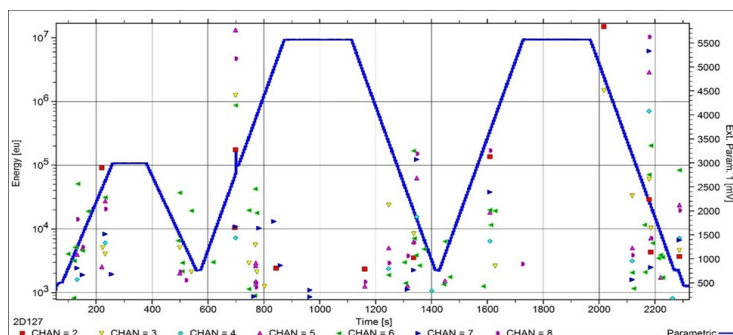


Fig. 4.18. Example of a graph of the dependence of the amplitude of AE signals on the time during a stepped static loading with shelves (with an operating time of 1,000,000 loading cycles).

For subsequent confirmation of the time of formation of the fatigue crack, periodically every 1,000 thousand cycles, a marker loading mode was made with a load 50 % lower than the working one for stage No. 2 for 15 minutes. The marker mode provides the possibility of visual fixation of the time of the formation of a fatigue crack during subsequent fractographic studies of the microrelief of fracture destruction.

Figure 4.19 shows the results of the current graphs of the dependencies of the change in the total AE account on the number of load cycles separately for each channel.

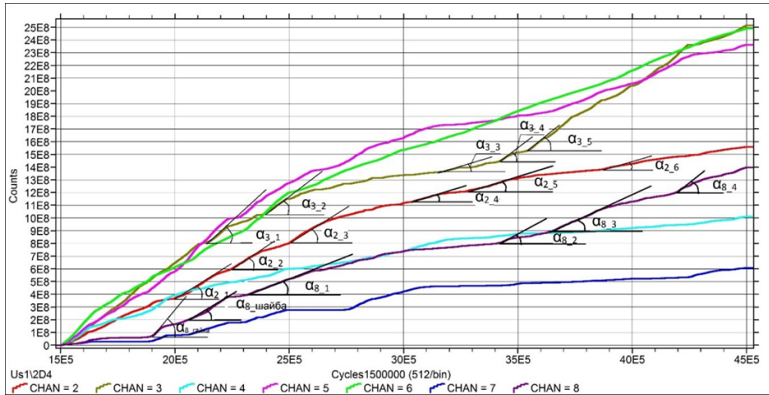


Fig. 4.19. General graph of the dependence of the change in the total AE account on the number of cycles of load application by channels at the operating time stage from 1.5 to 4.5 million cycles (the second loading mode).

It follows from the graph that the change in the total account of the AE is not stationary. The appearance at various stages of loading of sufficiently pronounced α criteria should indicate the occurrence and development of damage in the structure. The nature of the damage was established based on further analysis and the comparison of AE measurement data with the results of subsequent visual inspection.

Along with the certification tests, assessments of the prospects for using the implemented piezoceramic transducers as sensors for passive ultrasonic monitoring during fatigue tests of full-scale structures were carried out. The peculiarity lies in the fact that the intensity of the load of the structure during testing, as a rule, is higher than in operation. The “equivalent duration” shall be several times the lifetime of the aircraft in service. The results obtained here make it possible to make an optimal choice of the parameters of piezoelectric transducers for their use in passive monitoring: functional and strength properties of piezoceramics, geometric dimensions, modal characteristics, method of introduction into the design, and method of protection against external influences.

5. GENERAL CONCLUSIONS

The analysis and solutions to several relevant problems of operability and reliability of ultrasonic structural health monitoring mainly related to using the current information of embedded piezoceramic transducers working in both active and passive regimes of damage detection are presented in the Doctoral Thesis.

The following tasks had to be solved to achieve the formulated general aim:

1. There is a completed analysis of the piezoceramic transducers strength using Internet resources, experimental data, and finite element analysis (FEA) of stress state for typical installation and typical operational loading. Recommendations for preventing damage to the static and cyclical load are made.
2. Estimation of EMI as the primary method of fatigue crack detection is made. The comparison of properties of alternative indices of damage has been done. The detailed procedure of measurement data processing is developed.
3. The crack open/close effect on EMI is investigated and the suitability of this effect for the crack-type damage detection is estimated.
4. Two improved damage indices for the crack-type damage detection by the guided wave technology are developed. Both damage indices (RMSD and time-of-flight) are based on the convolution of the response signal for which the excitation signal is used as the mother function.
5. The example of application of reference-free virtual system of SHM is demonstrated (for the skin of hermetic fuselage of the passenger aircraft). It can be concluded that a hermetic fuselage structure is a very convenient field for application of ultrasonic technology of structural health monitoring which uses the crack open/close effect.
6. The application of piezoelectrical transducer for load monitoring is analysed. The fatigue damage index using the rain-flow method of operational load counting, fatigue test data and simulation outcome is developed. The allowable value of the index is mainly defined by the safety factor.
7. A probabilistic model of strength for SHM of lifetime by using load monitoring is presented. Using this model, it is possible to solve the problem of the proper determination of the maximum allowable parameter or diagnostic sign for indication in the cockpit when the predetermined limit of its actual value is known in advance.
8. The application of acoustic emission (AE) as a passive ultrasonic method is analysed in respect of its use in the laboratory test of aircraft full-scale components. Basic technical requirements of bench test for real time full-scale testing of helicopters are formulated. The results obtained from the bench tests can be used in testing the calculations of the resources of helicopter elements according to the criteria of short-term strength and endurance.

6. BIBLIOGRAPHY

1. Alfredo Guemes, "SHM Technologies and Applications in Aircraft Structures", 5th International Symposium on NDT in Aerospace, 13–15th November 2013, Singapore, https://www.ndt.net/article/aero2013/content/papers/61_Guemes
2. Tanimoto, T., Yamamoto, K., & Morii, T, "Nonlinear Stress-Strain Behavior of Piezoelectric Ceramics under Tensile Loading", Proceedings of the 9th IEEE International Symposium on Applications of Ferroelectrics, IEEE (1994): 394–397, IEEE Xplore.
3. Bin Lin, Victor Giurgiutiu, Patrick Pollock, Buli Xu, and James Doane, "Durability and Survivability of Piezoelectric Wafer Active Sensors on Metallic Structure", AIAA Journal 201048:3, pp. 635–643, <https://doi.org/10.2514/1.44776>
4. C. Meisner, C. Stolz, F. Hofmann, "Durability assessment of PZT-transducers for guided wave based shm systems using tensile static and fatigue tests", Publication: 7th International Symposium on NDT in Aerospace, 16–18 Nov. 2015, Bremen, Germany (AeroNDT 2015), www.ndt.net/search/docs.php?id=18940
5. I. Pavelko, "Research on the Protection of Piezoceramics Transducers from the Destruction by Mechanical Loading", Int. Virtual J. for Science, Technics and Innovations for the Industry, Issue 7 (2010), 17–21.
6. I. Pavelko, V. Pavelko, S. Kuznetsov, E. Ozolinsh, I. Ozolinsh, H. Pfeiffer, M. Wevers, "Problems of structural health monitoring of aircraft component", The proceeding of 27th Congress of the International Council of the Aeronautical Sciences, Nice, France, 19–24 September 2010, (Section 10, ICAS 2010-10.6.1).
7. C. T. Sun, "Fracture and fatigue of piezoceramics under mechanical and electrical loads", Durability 2000 Proceedings of the Durability Workshop, Berkeley, California, 26–27 October 2000. 2001, pp. 231–244.
8. Liang, C., Sun, F. P., and Rogers, C. A. Coupled electro-mechanical analysis of adaptive material system-determination of the actuator power consumption and system energy transfer. Journal of Intelligent Material Systems and Structures, 5, pp. 12–20, 1994.
9. Sun, F. P., Liang, C., and Rogers, C. A. Experimental modal testing using piezoceramic patches as collocated sensors-actuators. Proceeding of the 1994 SEM Spring Conference and Exhibits, Baltimore, MI, June 6–8, 1994.
10. Sun, F. P., Chaudhry, Z., Rogers, C. A., and Majmundar, M. Automated real-time structure health monitoring via signature pattern recognition. Proceedings, SPIE North American Conference on Smart Structures and Materials, Vol. 2443. San Diego, CA, 26 Feb.–3 March 1995, pp. 236–247.
11. Chaudhry, Z., Sun, F. P., and Rogers, C. A. Health monitoring of space structures using impedance measurements. Fifth International Conference on Adaptive Structures, Sendai, Japan, 5–7 December 1994, pp. 584–591.
12. Chaudhry, Z., Joseph, T., Sun, F., and Rogers, C. Local-area health monitoring of aircraft via piezoelectric actuator/sensor patches. Proceedings, SPIE North American Conference on Smart Structures and Materials, Vol. 2443. San Diego, CA, 26 Feb.–3 March 1995, pp. 268–276.
13. Ayres, T., Chaudhry, Z., and Rogers, C. Localized health monitoring of civil infrastructure via piezoelectric actuator/sensor patches. Proceedings, SPIE's 1996 Symposium on Smart Structures and Integrated Systems, SPIE, Vol. 2719, pp. 123–131, 1996.
14. Giurgiutiu, V., and Rogers, C. A. Electro-mechanical (E/M) impedance method for structural health monitoring a non-destructive evaluation. Int. Workshop on Structural Health Monitoring Stanford University, CA, 18–20, pp. 433–444, September 1997.
15. Giurgiutiu, V., and Zagrai, A. Characterization of piezoelectric wafer active sensors. Journal of Intelligent Material Systems and Structures, 11(12), pp. 959–976, 2000.
16. Giurgiutiu, V., Zagrai, A., and Bao, J. (2002). Piezoelectric wafer active sensors (PWAS), USC IPMO Invention Disclosure #00330/2002.
17. Victor Giurgiutiu, Andrei Zagrai, and Jing Jing Bao. Piezoelectric Wafer Embedded Active Sensors for Aging Aircraft Structural Health Monitoring. SHM, 2002, Vol.

1(1): 0041–61.

18. V. Pavelko. New applications of a model of electromechanical impedance for SHM. In: Health Monitoring of Structural and Biological Systems 2014, United States of America, San Diego, 9–13 March 2014. Bellingham: SPIE, 2014, pp. 90640Y-1-90640Y-15. ISBN 978-0-8194-9990-5. Available from: doi:10.1117/12.2044260
19. W. Thomson, “On the Electro-Dynamic Qualities of Metals: Effects of Magnetization on the Electric Conductivity of Nickel and of Iron,” Proceedings of the Royal Society of London, Vol. 8, 1856, pp. 546–550. <http://dx.doi.org/10.1098/rspl.1856.0144>
20. H. Tomlinson. The influence of stress and strain on the action of physical forces. Phil. Trans. Vol. 174, pp. 1–172 1883 <https://doi.org/10.1098/rstl.1883.0001>
21. H. Rolnick. Tension Coefficient of Resistance of Metals. Phys. Rev. 36(3), 506–512 (1930) DOI:<https://doi.org/10.1103/PhysRev.36.506>
22. J. W. Cookson. Theory of piezo-resistive effect. Phys. Rev. 47(2), 194–195 (1935) DOI: <https://doi.org/10.1103/PhysRev.47.194.2>
23. M. A. Radhika, V. G. M. Annamdas, “Experimental studies on structural load monitoring using piezoelectric transducer based electromechanical impedance method”, Scientific Journal of Review (2013), 2(1). ISSN 2322-2433.
24. M. Urbaha, K. Carjova, P. Nagaraj, V. Turko, “Requirements for Helicopter’s Planer Construction Fatigue Testing”, Proceedings of 22nd International Scientific Conference. Transport Means 2018,
25. J. W. Cookson, “Theory of piezo-resistive effect”, Phys. Rev. 47(2) 194–195 (1935), <https://doi.org/10.1103/PhysRev.47.194.2>
26. H. Rolnick, “Tension Coefficient of Resistance of Metals”, Phys. Rev. 36(3), 506 – 512 (1930), <https://doi.org/10.1103/PhysRev.36.506>
27. C. S. Smith, “Piezoresistance effect in germanium and silicon”, Phys. Rev. 94(1), 42–49 (1954), <http://dx.doi.org/10.1103/PhysRev.94.42>
28. Joseph C. Doll, Beth L. Pruitt, “Piezo resistor Design and Applications (Microsystems and Nano systems)” Springer, 2013. 245 p, Doi 10.1007/78-1-4614-8517-9.
29. Airworthiness of Aircraft. Annex 8 to the Convention on International Civil Aviation. ICAO. ISBN 978-92-9231-518-4.
30. M. Miner. Cumulative Damage in Fatigue. J. Appl. Mech. Sep 1945, 12(3): A159–A164 (6 p.) <https://doi.org/10.1115/1.4009458>
31. Jaap Schijve. Fatigue of Structures and Materials. Springer, 2010. 621 pages.
32. Schütz, D., and Lowak, H., The application of the standardized test program for the fatigue life estimation of transport aircraft wing components. Proc. ICAF Symp., Lausanne, Paper 3.64 (1975).
33. Schütz, W., Standardized stress-time histories: An overview. Development of Fatigue Load Spectra, STP 1006, ASTM (1989), pp. 3–16.
34. Matsuishi, M., and Endo, T., Fatigue of metals subjected to varying stress – Fatigue lives under random loading. Preliminary Proc. of the Kyushu District Meeting, The Japan Society of Mechanical Engineers (1968), pp. 37–40 [in Japanese].
35. Burns, A., Fatigue loadings in flight: Loads in the tailplane and fin of a Varsity. A.R.C. Technical Report C.P.256. London (1956).
36. Mil, M.L. et al. (1967) “Vertoleti. Raschet I projektirovanie (Helicopters. Calculations and engineering)”. Book 2. Kolebanija i dinamičeskaja pročnostj (Oscillations and dynamic strength). Moscow: Machinostroenie, 424.
37. Dimitrios G. Aggelis, Markus G. R. Sause, Pawel Packo, Rhys Pullin, Steve Grigg, Tomaž Kek, and Yu-Kun Lai, “Acoustic Emission”, (2021) Structural Health Monitoring Damage Detection Systems for Aerospace, Springer Aerospace Technology, https://www.ndt.net/article/ndtreview/papers/Aggelis2021_Chapter_AcousticEmission.pdf



Pavithra Nagaraj was born in Chitradurga, Bangalore City, India, in 1985. She received a Bachelor's degree in Aeronautics from VSM Aerospace Bangalore, India, in 2009, a qualification of aircraft maintenance engineer (Avionics licensed) from DGCA India in 2008 and a Professional Master's degree in Aviation Transport from Riga Technical University in 2017. Since 2017, she has been a research assistant with the Aircraft Structures Laboratory of RTU. She has participated in 2 European projects. She is also a teaching assistant at the Aeronautical institute of MTAF, RTU. From 2010 to 2015, she was an avionics licensed maintenance engineer at Zephyr Aerospace Bangalore, ADE, (Defence laboratories) DRDO. She has participated in 6 defence projects in India. From 2007 to 2008, she was a trainee technician in the helicopter division of Deccan Chartered. Her research interests include NDT, acoustic emission, aircraft structures, vibro-acoustics, helicopter structures, numerical analysis, composites, and UAVs.